LETTER

doi:10.1038/nature23669

Identification of CMTM6 and CMTM4 as PD-L1 protein regulators

Riccardo Mezzadra[1]*, Chong Sun[1]*, Lucas T. Jae[2]†*, Raquel Gomez-Eerland[1], Evert de Vries[3], Wei Wu[4,5], Meike E. W. Logtenberg[1], Maarten Slagter[1,6], Elisa A. Rozeman[1,7], Ingrid Hofland[8], Annegien Broeks[8], Hugo M. Horlings[9], Lodewyk F. A. Wessels[6], Christian U. Blank[1,7], Yanling Xiao[3], Albert J. R. Heck[4,5], Jannie Borst[3], Thijn R. Brummelkamp[2,10,11] & Ton N. M. Schumacher[1]

The clinical benefit for patients with diverse types of metastatic cancers that has been observed upon blockade of the interaction between PD-1 and PD-L1 has highlighted the importance of this inhibitory axis in the suppression of tumour-specific T-cell responses[1–9]. Notwithstanding the key role of PD-L1 expression by cells within the tumour micro-environment, our understanding of the regulation of the PD-L1 protein is limited[10–15]. Here we identify, using a haploid genetic screen, CMTM6, a type-3 transmembrane protein of previously unknown function, as a regulator of the PD-L1 protein. Interference with CMTM6 expression results in impaired PD-L1 protein expression in all human tumour cell types tested and in primary human dendritic cells. Furthermore, through both a haploid genetic modifier screen in CMTM6-deficient cells and genetic complementation experiments, we demonstrate that this function is shared by its closest family member, CMTM4, but not by any of the other CMTM members tested. Notably, CMTM6 increases the PD-L1 protein pool without affecting *PD-L1* (also known as *CD274*) transcription levels. Rather, we demonstrate that CMTM6 is present at the cell surface, associates with the PD-L1 protein, reduces its ubiquitination and increases PD-L1 protein half-life. Consistent with its role in PD-L1 protein regulation, CMTM6 enhances the ability of PD-L1-expressing tumour cells to inhibit T cells. Collectively, our data reveal that PD-L1 relies on CMTM6/4 to efficiently carry out its inhibitory function, and suggest potential new avenues to block this pathway.

Antibodies that block the PD-1–PD-L1 axis are currently evaluated in approximately 800 clinical studies and have been approved for seven different tumour types. In addition, expression of PD-L1 on either tumour cells or on tumour-infiltrating immune cells identifies patients that are more likely to respond to these therapies[16,17]. In view of the limited understanding of the regulation of PD-L1 expression, we set out to identify PD-L1 protein regulators through genetic screening. Interferon-γ (IFNγ)-treated haploid HAP1 cells[18,19] express high levels of PD-L1 on the cell surface (Extended Data Fig. 1a). On the basis of this observation, we performed a fluorescence-activated cell sorting (FACS)-based haploid genetic screen for PD-L1 modulators in IFNγ-treated HAP1 cells (Fig. 1a, experimental design as in ref. 20). The entire IFNγ receptor (IFNγR)-signalling pathway[21] plus IRF1, a known regulator of PD-L1 upon IFNγ exposure[10], were identified as strong hits (Fig. 1a and Supplementary Table 1), demonstrating the validity of the screen setup. In addition, the PD-L1 gene itself (*CD274*) showed a strikingly different integration pattern in PD-L1^{high} and PD-L1^{low} cells. Specifically, whereas PD-L1^{low} cells showed the expected enrichment of integrations towards the 5′ end of the gene, a strong enrichment of integrations in intron 5 and 6 was observed in PD-L1^{high} cells (Extended Data Fig. 1b), fully consistent with the recently described negative regulatory role of the PD-L1 3′ untranslated region (UTR)[11] (Extended Data Fig. 1c).

In addition to the above hits, we identified CMTM6 (CKLF (chemokine-like factor)-like MARVEL transmembrane domain containing family member 6) as one of the most significant hits within PD-L1^{low} cells. CMTM6 was not observed in a similar screen for regulators of IRF1 protein levels[20], suggesting that its role was independent of the IFNγR pathway. CMTM6 is a ubiquitously expressed transmembrane protein that belongs to a family of eight MARVEL-domain-containing proteins[22] for which no clear function has been described. Transcriptome analysis of tumour samples in The Cancer Genome Atlas (TCGA) showed CMTM6 expression in all of the analysed samples distributed across 30 cancer types, and showed that RNA expression levels of *CMTM6* and *CD274* are weakly correlated in the majority of tumour types (Extended Data Fig. 2). Short hairpin RNA (shRNA)-mediated knockdown of *CMTM6* in HAP1 cells reduced IFNγ-induced PD-L1 expression approximately twofold compared to control (Fig. 1b, c). To assess whether CMTM6 also influences PD-L1 cell surface levels beyond the HAP1 system, we examined the effect of CMTM6 knockdown in a series of tumour lines. In A375 melanoma cells, which only show detectable PD-L1 expression after IFNγ exposure, CMTM6 knockdown prevented IFNγ-induced PD-L1 expression to a large extent (Fig. 2a-c, reduction up to 11-fold). CMTM6-deficient A375 clones generated with CRISPR–Cas9 likewise showed reduced cell surface and overall PD-L1 protein levels, whereas lentiviral reconstitution of CMTM6 reverted this phenotype (Fig. 2d, e). In the 8505C thyroid cancer cell line, which has a high basal level of PD-L1 expression, both steady state and IFNγ-induced PD-L1 cell surface and total protein levels were substantially reduced by CMTM6 knockdown (Fig. 2f, g, up to seven- and fivefold, respectively). In total, we assessed the effect of CMTM6 knockdown in 12 human tumour lines, representing melanoma (Fig. 2a–c and Extended Data Fig. 3a–d), thyroid cancer (Fig. 2f, g), colorectal cancer (Extended Data Fig. 3e, f, i, k), lung cancer (Extended Data Fig. 3l, n–p) and chronic myeloid leukaemia (Fig. 1b, c). In addition, we also tested the effect of CMTM6 knockdown in three short-term cultures of melanoma xenografts (Extended Data Fig. 3q). In these different cell systems, we consistently observed decreased expression of PD-L1 (between 2- and 11-fold) upon

[1]Division of Molecular Oncology & Immunology, The Netherlands Cancer Institute, Plesmanlaan 121, 1066 CX Amsterdam, The Netherlands. [2]Division of Biochemistry, The Netherlands Cancer Institute, Plesmanlaan 121, 1066 CX Amsterdam, The Netherlands. [3]Division of Tumor Biology & Immunology, The Netherlands Cancer Institute, Plesmanlaan 121, 1066 CX Amsterdam, The Netherlands. [4]Biomolecular Mass Spectrometry and Proteomics, Bijvoet Center for Biomolecular Research and Utrecht Institute for Pharmaceutical Sciences, Padualaan 8, 3584 CH Utrecht, The Netherlands. [5]Netherlands Proteomics Centre, Padualaan 8, 3584 CH Utrecht, The Netherlands. [6]Division of Molecular Carcinogenesis, The Netherlands Cancer Institute, Plesmanlaan 121, 1066 CX Amsterdam, The Netherlands. [7]Division of Medical Oncology, The Netherlands Cancer Institute, Plesmanlaan 121, 1066 CX Amsterdam, The Netherlands. [8]Core Facility Molecular Pathology & Biobanking, Division of Pathology, The Netherlands Cancer Institute, Plesmanlaan 121, 1066 CX Amsterdam, The Netherlands. [9]Division of Pathology, The Netherlands Cancer Institute, Plesmanlaan 121, 1066 CX Amsterdam, The Netherlands. [10]CeMM Research Center for Molecular Medicine of the Austrian Academy of Sciences, 1090 Vienna, Austria. [11]Cancergenomics.nl, Plesmanlaan 121, 1066 CX Amsterdam, The Netherlands. †Present address: Gene Center and Department of Biochemistry, Ludwig-Maximilians-Universität München, Feodor-Lynen-Straße 25, 81377 Munich, Germany.
*These authors contributed equally to this work.

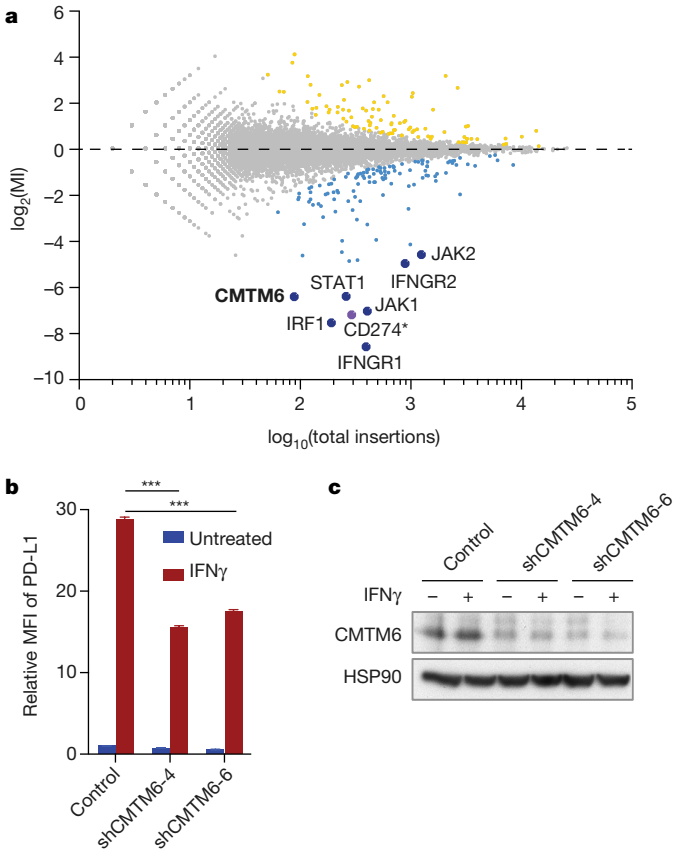

Figure 1 | Identification of CMTM6 as a modulator of PD-L1 expression. a, Flow-cytometry-based screen for modulators of PD-L1 cell surface expression in HAP1 cells. Dots represent individual genes; *x* axis indicates the number of disruptive insertions per gene; *y* axis shows the frequency of independent insertions in the PD-L1^{high} channel over the frequency of insertions in the PD-L1^{low} channel for each gene. Light-blue and orange dots indicate genes with significant enrichment of insertions (FDR-corrected $P < 10^{-6}$)[27] within the PD-L1^{low} and PD-L1^{high} populations, respectively. Dark-blue circles indicate known components of the IFNγR-signalling pathway plus IRF1 and CMTM6 (in bold). The purple dot represents PD-L1 (*CD274**) when excluding integrations downstream of exon 5 (Refseq identifier NM_014143.3). See https://phenosaurus.nki.nl for interactive graphs. **b**, Relative PD-L1 cell-surface expression in control or independent CMTM6-knockdown HAP1 cells with or without IFNγ exposure. **c**, Validation of CMTM6 knockdown by western blot. Data are representative of one (**a**) or at least three (**b**, **c**) independent experiments, and were analysed by unpaired *t*-test (**b**). Data represent mean ± s.d. of triplicates (**b**). ***$P < 0.001$. MFI, median fluorescence intensity; MI, mutation index.

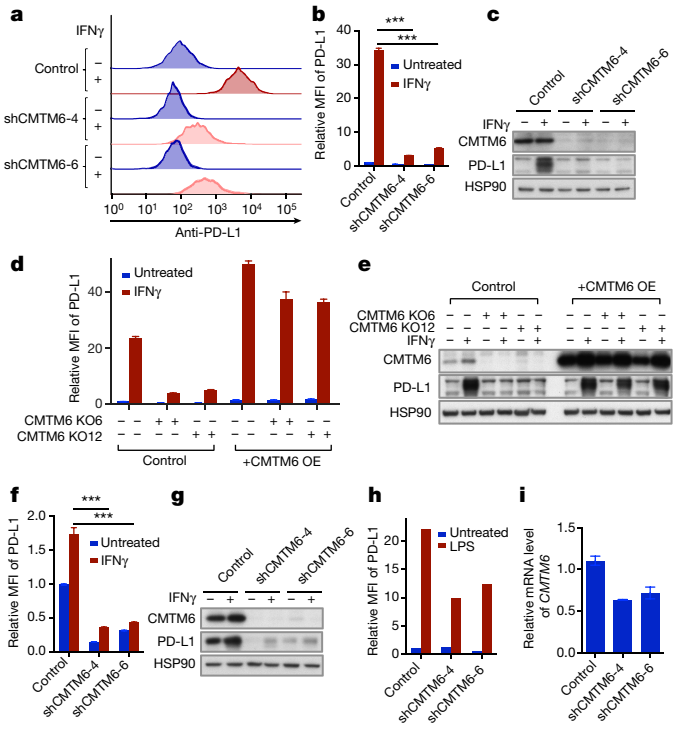

Figure 2 | CMTM6 regulates PD-L1 expression in different tumour types and primary dendritic cells. a, **b**, Relative PD-L1 cell surface expression in control or independent CMTM6-knockdown (shCMTM6-4, shCMTM6-6) A375 melanoma cells with or without IFNγ exposure. **c**, Western blot analysis of CMTM6 and PD-L1 expression in control or independent CMTM6-knockdown A375 melanoma cells with or without IFNγ exposure. **d**, **e**, Flow cytometry (**d**) and western blot (**e**) analysis of PD-L1 expression in parental, CMTM6-deficient, CMTM6-overexpressing and CMTM6-reconstituted A375 melanoma cells. **f**, Relative PD-L1 cell surface expression in control or independent CMTM6-knockdown (shCMTM6-4, shCMTM6-6) 8505C thyroid cancer cells with or without IFNγ exposure. **g**, Western blot analysis of CMTM6 and PD-L1 expression in control or independent CMTM6-knockdown 8505C thyroid cancer cells with or without IFNγ exposure. **h**, Flow cytometry analysis of PD-L1 expression in control or independent CMTM6-knockdown primary bone marrow progenitor-derived dendritic cells with or without LPS exposure. **i**, Knockdown efficiency of CMTM6 in primary bone marrow progenitor-derived dendritic cells. Data are representative of at least three (**a**–**g**) or two (**h**, **i**) independent experiments and were analysed by unpaired *t*-test (**b**, **f**). Data represent mean ± s.d. of triplicates (**b**, **d**, **f**, **i**). ***$P < 0.001$. MFI, median fluorescence intensity.

knockdown of CMTM6. Reduced PD-L1 cell surface levels were likewise observed when cells were stained with recombinant PD-1–Fc protein (Extended Data Fig. 3h, j, m). PD-L1 can be expressed by both cancer cells and infiltrating immune cells, and PD-L1 expression on immune cells may contribute to T-cell inhibition[16,17]. To assess whether CMTM6 also influences PD-L1 levels in primary human dendritic cells, we generated dendritic cells from human bone marrow progenitors[23]. Comparison of lipopolysaccharide (LPS)-induced PD-L1 expression in control and CMTM6-knockdown dendritic cells showed that partial knockdown of CMTM6 resulted in a partial reduction of PD-L1 cell-surface levels (Fig. 2h, i).

The above data establish CMTM6 as a modulator of PD-L1 protein levels. Whereas in some tumour lines, the effect of CMTM6 knockdown is strong (for example, A375, 8505C), in others it is moderate (for example, HAP1), suggesting the possible existence of (an) additional regulator(s). We therefore generated CMTM6-knockout HAP1 cells and performed a modifier screen, with the aim of identifying genetic factors that selectively regulate PD-L1 in the absence of CMTM6. Consistent with the primary screen, genes mediating IFNγR signalling were prominent hits. As expected, in this setting, integrations within the *CMTM6* locus were no longer enriched within the PD-L1^{low} cell population (Fig. 3a and Supplementary Table 2). In CMTM6-deficient HAP1 cells, CMTM4, another member of the CMTM family with 55% homology to CMTM6, was identified as a positive regulator of PD-L1 expression (Fig. 3a). Notably, although CMTM4 is a highly significant hit in CMTM6-deficient HAP1 cells (36.7-fold, false discovery rate (FDR)-corrected $P \leq 10^{-314}$), it is not in CMTM6-proficient HAP1 cells (0.9-fold, FDR-corrected $P = 0.94789$), suggesting that in this system, CMTM4 functions as a back-up regulator of PD-L1 expression.

To validate these data, we transduced H2030 cells, in which CMTM6 depletion modestly suppresses PD-L1 expression and CMTM4 is highly expressed, with shRNAs against *CMTM4* and *CMTM6*, either separately or in combination. In these cells, silencing of *CMTM6* led to repression of IFNγ-induced PD-L1 expression that was further

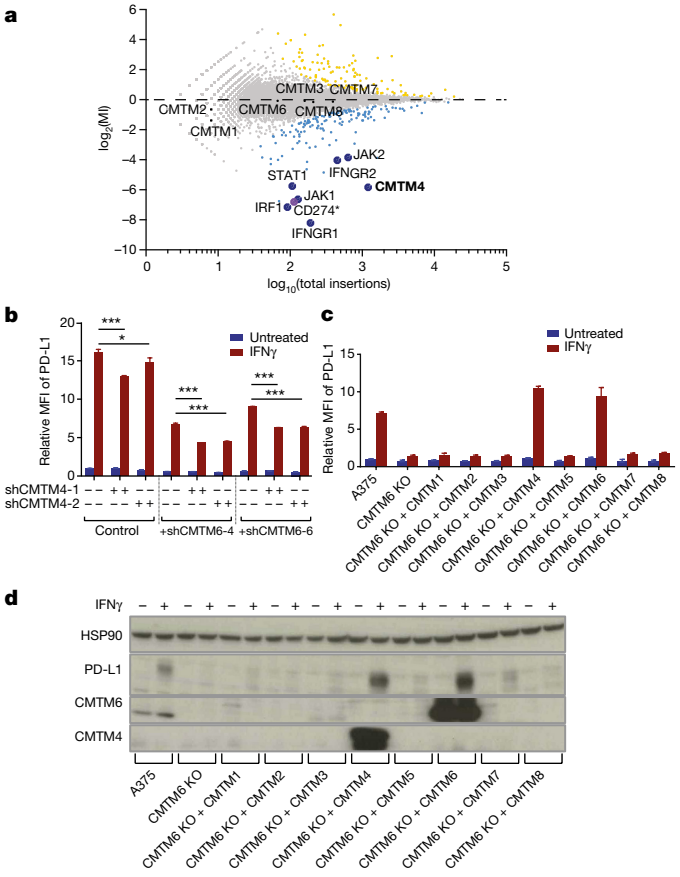

Figure 3 | Identification of CMTM4 as a second PD-L1 regulator. **a**, Haploid genetic screen for modulators of PD-L1 cell surface expression in CMTM6-deficient HAP1 cells. **b**, PD-L1 surface expression in parental, CMTM6-knockdown, CMTM4-knockdown or double-knockdown H2030 cells with or without IFNγ exposure. **c**, **d**, Flow cytometry (**c**) and western blot (**d**) analysis of PD-L1 expression in parental A375, CMTM6-knockout A375 cells and CMTM6-knockout A375 cells reconstituted with the indicated CMTM family member with or without IFNγ exposure. Data are representative of one (**a**), two (**b**) or three (**c**, **d**) independent experiments and were analysed by unpaired *t*-test (**b**). Data represent mean ± s.d. of triplicates (**b**, **c**). $*P < 0.05$; $***P < 0.001$. KO, knockout; MFI, median fluorescence intensity; MI, mutation index.

enhanced when *CMTM4* was simultaneously targeted (Fig. 3b and Extended Data Fig. 4a). More directly, ectopic expression of CMTM4 could fully restore IFNγ-induced PD-L1 expression in CMTM6-knockout cells (Extended Data Fig. 4b, c). To understand whether regulation of PD-L1 expression is a specific property of CMTM6 and CMTM4, we individually introduced Flag-tagged versions of all CMTM family members into CMTM6-deficient A375 cells. In contrast to what was observed upon CMTM6 and CMTM4 introduction, expression of other CMTM members (detected for CMTM1, CMTM3, CMTM5 and CMTM7; Extended Data Fig. 4d, e) did not induce a substantial increase in PD-L1 expression, as assessed by either flow cytometry or western blot analysis (Fig. 3c, d).

To study the mechanism by which CMTM6 regulates PD-L1 levels, we first assessed the relationship between CMTM6 expression and *PD-L1* mRNA levels. Comparison of *PD-L1* mRNA levels and cell-surface protein levels at different time points after IFNγ stimulation revealed that whereas CMTM6 depletion greatly reduced PD-L1 cell-surface levels, induction of *PD-L1* mRNA by IFNγ was not substantially altered (Fig. 4a, b and Extended Data Fig. 5d). Notably, both in cell lines (Extended Data Fig. 5a) and in primary dendritic cells (Extended Data Fig. 5b, c), levels of MHC-I and PD-L2 protein were not significantly affected by CMTM6 inhibition, indicating that although CMTM6 regulates PD-L1 at the protein level, it is not a general regulator of protein translation or stability.

To determine where in the PD-L1 protein life cycle CMTM6 exerts its effect, CMTM6-deficient and CMTM6-overexpressing A375 cells were transduced with a V5-tagged PD-L1 gene. Immunoprecipitation of PD-L1–V5 at different time points after a 1-h ^{35}S pulse labelling demonstrated a much more rapid decay of PD-L1 in the absence of CMTM6 (fraction PD-L1 remaining at $t = 6$ h; 94% versus 8%; Fig. 4c and Extended Data Fig. 5e). Notably, acquisition of PD-L1 resistance to deglycosylation by endoglycosidase H, was equally efficient in both cell populations, indicating that CMTM6 influences PD-L1 protein fate after egress from the endoplasmic reticulum (Extended Data Fig. 5f).

To reveal the cellular localization of endogenous CMTM6, we performed mass spectrometry analysis of different subcellular fractions, demonstrating that endogenous CMTM6 is predominantly present within the plasma membrane fraction (Extended Data Fig. 6a) Immunohistochemical analysis confirmed the presence of CMTM6 at the cell membrane (Extended Data Fig. 6b). Furthermore, immunohistochemical analysis of nine melanomas revealed CMTM6 protein expression in human tumours, and also showed that PD-L1 staining in eight of these samples was restricted to areas with clear CMTM6 expression (Extended Data Fig. 6c). Similarly, in three out of five PD-L1$^+$ lung cancer samples, we observed PD-L1 localization in CMTM6$^+$ areas.

A hypothesis arising from the above data is that CMTM6 and PD-L1 could interact molecularly. To test this, we performed immunoprecipitation of PD-L1 followed by western blot analysis of CMTM6, and vice versa. In lysates from A375 cells or 8505C cells, anti-PD-L1 antibody co-immunoprecipitated CMTM6. Likewise, PD-L1 was present in anti-CMTM6 immunoprecipitates. As expected, co-immunoprecipitation of PD-L1 and CMTM6 in A375 was dependent upon PD-L1 induction by IFNγ. As a further control for antibody specificity, co-immunoprecipitation of both CMTM6 and PD-L1 was abrogated upon gene inactivation of the partner molecule (Fig. 4d and Extended Data Fig. 7a, b). Co-immunoprecipitation was likewise observed for PD-L1 and CMTM4, and CMTM4 and CMTM6 (Extended Data Fig. 7c, d).

To understand how CMTM6 influences PD-L1 degradation, wild-type, CMTM6-knockout, and CMTM6-overexpressing A375 were transduced with a V5-tagged PD-L1 gene and ubiquitination of PD-L1 was analysed. In the absence of CMTM6, the amount of ubiquitinated PD-L1 was increased, despite the overall lower PD-L1 levels (Fig. 4e and Extended Data Fig. 8a), suggesting that CMTM4/6 may protect PD-L1 from ubiquitination. Intriguingly, STUB1, an E3 ubiquitin ligase that has, among others, been implicated in the degradation of Foxp3 in regulatory T cells[24], was identified as a negative regulator of PD-L1 expression in both haploid genetic screens (Extended Data Fig. 8b, c). To assess whether STUB1 affects PD-L1 degradation, we disrupted STUB1 in either CMTM6-proficient or -deficient A375 cells. Deletion of STUB1 resulted in a stronger increase in PD-L1 levels in CMTM6-deficient than in CMTM6-proficient cells, identifying STUB1 as an E3 ligase that causes destabilization of PD-L1 (Fig. 4f, g), either directly, by modification of lysines in the PD-L1 cytoplasmic domain, or indirectly. Consistent with the model that CMTM6 may protect PD-L1 by preventing ubiquitination, cell-surface levels of PD-L1–PD-L2 fusion proteins are only influenced by CMTM6 when carrying the PD-L1 transmembrane and intracellular domain (Extended Data Fig. 8d, e). Exploiting the fact that CMTM6 and PD-L2 do not show detectable association (Extended Data Fig. 8f), we also used PD-L1–PD-L2 fusion proteins to demonstrate that the PD-L1 transmembrane domain is required for efficient interaction (Extended Data Fig. 8g). In line with the role of the PD-L1 transmembrane and intracellular domain in CMTM6-mediated stabilization, orientation mapping of CMTM6 revealed that a large part of the molecule is located within the cytosol and cell membrane (Extended Data Fig. 9).

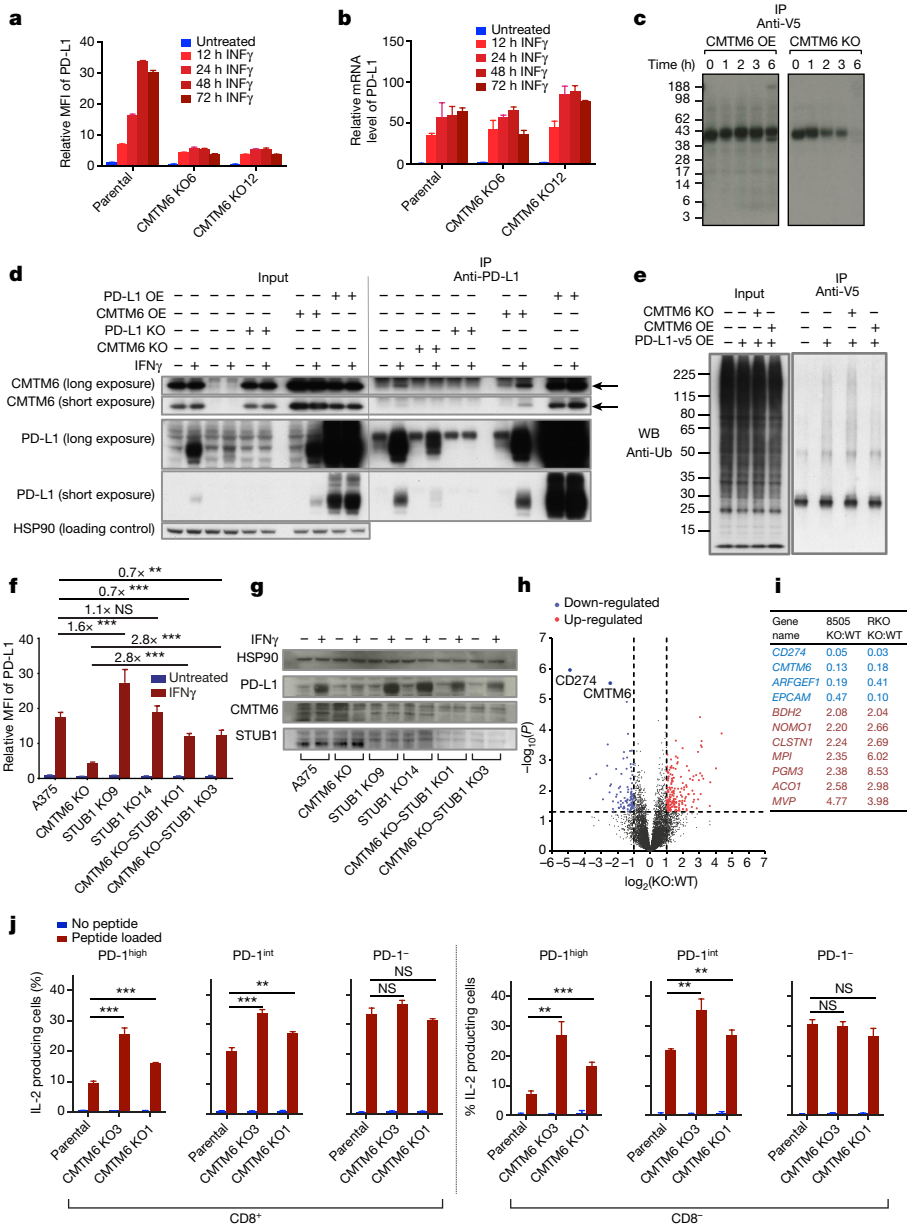

Figure 4 | CMTM6 forms a molecular partner of PD-L1 and regulates PD-L1 protein stability. a, **b**, Time course of PD-L1 surface protein (**a**) or mRNA (**b**) levels in A375 cells upon IFNγ exposure. **c**, SDS–PAGE analysis of anti-V5 immunoprecipitates from V5–PD-L1 overexpressing CMTM6-knockout or CMTM6-overexpressing A375 cells at different time points after ^{35}S methionine/cysteine labelling. **d**, Immunoblots of lysates or anti-PD-L1 immunoprecipitates from the indicated A375 melanoma cells with or without IFNγ exposure. Arrows indicate CMTM6. **e**, Immunoblots of lysates or anti-V5 immunoprecipitates from V5-PD-L1 overexpressing parental, CMTM6-knockout or CMTM6-overexpressing A375 cells. **f**, **g**, PD-L1 surface protein (**f**) or lysate immunoblots (**g**) of parental, CMTM6-knockout, STUB1-knockout or double-knockout A375 cells. Numbers in **f** represent relative PD-L1 MFI. **h**, Comparative plasma membrane-fractionated mass spectrometry of four CMTM6-proficient and four CMTM6-deficient 8505C clones. **i**, Overview of proteins consistently found up- (red) or downregulated (blue) upon CMTM6 removal in both 8505C and RKO cells. **j**, IL-2 production by PD-1^{high}, PD-1^{int} and PD-1^{-} primary human T cells obtained by transduction with the MART-I-specific 1D3 TCR and PD-1, and co-cultured with unloaded or MART-I peptide-loaded parental or CMTM6-knockout 8505C cells. Data are representative of two (**a**, **b**), one (**c**, **h**) or three (**d**–**g**, **j**) independent experiments and were analysed by unpaired *t*-test (**f**, **j**). Data represent mean ± s.d. of triplicates (**a**, **b**, **f**, **j**). $^{**}P < 0.01$; $^{***}P < 0.001$; NS, not significant. KO, knockout; IP, immunoprecipitation; MFI, median fluorescence intensity; OE, overexpression; Ub, ubiquitin; WB, western blot.

In view of the broad RNA expression pattern of *CMTM6*, we assessed the effects of CMTM6 on the membrane proteome in an unbiased manner. Mass spectrometric analysis of a series of independent CMTM6-deficient and -proficient clones revealed that, both within the 8505C thyroid cancer cell line and the RKO colorectal cancer cell line, PD-L1 was the most significantly influenced hit (Fig. 4h, i and Extended Data Fig. 10a, b). Expression of PD-L1 affects T-cell responsiveness in a quantitative manner, with higher levels of PD-L1 expression leading to an increased impairment of T-cell survival and/or activity[11,25]. To determine whether CMTM6 influences PD-L1-mediated T-cell suppression, we incubated mixtures of MART-I T-cell receptor (TCR)-transduced T cells that expressed different levels of PD-1 with antigen-loaded CMTM6-deficient or -proficient 8505C or A375 cells. IL-2 production of PD-1^{int} and PD-1^{high} T cells upon encounter of CMTM6-proficient tumour cells was reduced relative to that of PD-1^{-} T cells. However, upon CMTM6 disruption in 8505C or A375 tumour cells, IL-2 production of PD-1-expressing T cells was significantly restored (Fig. 4j and Extended Data Fig. 10c–e).

Recent work has revealed a number of mechanisms of transcriptional and post-transcriptional (dys)regulation of the PD-L1 gene in tumour cells[10–15]. Here we identify CMTM6 and CMTM4 as regulators of PD-L1 protein stability. On the basis of the available data we conclude that CMTM6/4, the two most closely related members of the CMTM family (Extended Data Fig. 4f), influence PD-L1 expression across a range of cell types. Furthermore, the observations that (i) CMTM6 affects PD-L1 protein stability at late time points after biosynthesis; (ii) CMTM6, CMTM4 and PD-L1 interact, as shown by co-immunoprecipitation; and that (iii) CMTM6 is largely located at the cell surface, collectively suggest a model in which CMTM6 interacts with PD-L1 at the tumour cell surface and thereby protects it from degradation. In line with this model, CMTM6 influences the levels of PD-L1 ubiquitination and absence of the STUB1 E3 ubiquitin ligase partially reverts the CMTM6-knockout phenotype. Intriguingly, for one of the other CMTM family members, CMTM7, cell surface expression has been described in association with the B-cell receptor (BCR) complex, where it may contribute to BCR signalling[26]. It could be speculated that CMTM6 may also fulfil a similar role in the immunological synapse between T cells and tumour cells or antigen-presenting cells. Finally, the co-localization of PD-L1 and CMTM6 in human tumours and the observation that CMTM6 depletion ameliorates PD-L1-mediated T-cell suppression suggest a potential value of CMTM6/4 as therapeutic targets, either in isolation, or to enhance the effectiveness of the current PD-L1–PD-1 blocking therapies.

Online Content Methods, along with any additional Extended Data display items and Source Data, are available in the online version of the paper; references unique to these sections appear only in the online paper.

Received 13 December 2016; accepted 25 July 2017.
Published online 16 August 2017.

1. Topalian, S. L. *et al.* Safety, activity, and immune correlates of anti-PD-1 antibody in cancer. *N. Engl. J. Med.* **366,** 2443–2454 (2012).
2. Brahmer, J. R. *et al.* Safety and activity of anti-PD-L1 antibody in patients with advanced cancer. *N. Engl. J. Med.* **366,** 2455–2465 (2012).
3. Ansell, S. M. *et al.* PD-1 blockade with nivolumab in relapsed or refractory Hodgkin's lymphoma. *N. Engl. J. Med.* **372,** 311–319 (2015).
4. Powles, T. *et al.* MPDL3280A (anti-PD-L1) treatment leads to clinical activity in metastatic bladder cancer. *Nature* **515,** 558–562 (2014).
5. Garon, E. B. *et al.* Pembrolizumab for the treatment of non-small-cell lung cancer. *N. Engl. J. Med.* **372,** 2018–2028 (2015).
6. Le, D. T. *et al.* PD-1 blockade in tumors with mismatch-repair deficiency. *N. Engl. J. Med.* **372,** 2509–2520 (2015).
7. Motzer, R. J. *et al.* Nivolumab versus everolimus in advanced renal-cell carcinoma. *N. Engl. J. Med.* **373,** 1803–1813 (2015).
8. Nghiem, P. T. *et al.* PD-1 blockade with pembrolizumab in advanced Merkel-cell carcinoma. *N. Engl. J. Med.* **374,** 2542–2552 (2016).
9. Ferris, R. L. *et al.* Nivolumab for recurrent squamous-cell carcinoma of the head and neck. *N. Engl. J. Med.* **375,** 1856–1867 (2016).
10. Lee, S. J. *et al.* Interferon regulatory factor-1 is prerequisite to the constitutive expression and IFN-γ-induced upregulation of B7-H1 (CD274). *FEBS Lett.* **580,** 755–762 (2006).
11. Kataoka, K. *et al.* Aberrant PD-L1 expression through 3′-UTR disruption in multiple cancers. *Nature* **534,** 402–406 (2016).
12. Casey, S. C. *et al.* MYC regulates the antitumor immune response through CD47 and PD-L1. *Science* **352,** 227–231 (2016).
13. Dorand, R. D. *et al.* Cdk5 disruption attenuates tumor PD-L1 expression and promotes antitumor immunity. *Science* **353,** 399–403 (2016).
14. Li, C.-W. *et al.* Glycosylation and stabilization of programmed death ligand-1 suppresses T-cell activity. *Nat. Commun.* **7,** 12632 (2016).
15. Lim, S. O. *et al.* Deubiquitination and stabilization of PD-L1 by CSN5. *Cancer Cell* **30,** 925–939 (2016).
16. Herbst, R. S. *et al.* Predictive correlates of response to the anti-PD-L1 antibody MPDL3280A in cancer patients. *Nature* **515,** 563–567 (2014).
17. Ribas, A. & Hu-Lieskovan, S. What does PD-L1 positive or negative mean? *J. Exp. Med.* **213,** 2835–2840 (2016).
18. Carette, J. E. *et al.* Haploid genetic screens in human cells identify host factors used by pathogens. *Science* **326,** 1231–1235 (2009).
19. Carette, J. E. *et al.* Ebola virus entry requires the cholesterol transporter Niemann–Pick C1. *Nature* **477,** 340–343 (2011).
20. Brockmann, M. *et al.* Genetic wiring maps of single-cell protein states reveal an off-switch for GPCR signalling. *Nature* **546,** 307–311 (2017).
21. Platanias, L. C. Mechanisms of type-I- and type-II-interferon-mediated signalling. *Nat. Rev. Immunol.* **5,** 375–386 (2005).
22. Han, W. *et al.* Identification of eight genes encoding chemokine-like factor superfamily members 1–8 (*CKLFSF1–8*) by *in silico* cloning and experimental validation. *Genomics* **81,** 609–617 (2003).
23. Xiao, Y. *et al.* Identification of the common origins of osteoclasts, macrophages, and dendritic cells in human hematopoiesis. *Stem Cell Rep.* **4,** 984–994 (2015).
24. Chen, Z. *et al.* The ubiquitin ligase Stub1 negatively modulates regulatory T cell suppressive activity by promoting degradation of the transcription factor Foxp3. *Immunity* **39,** 272–285 (2013).
25. Wei, F. *et al.* Strength of PD-1 signaling differentially affects T-cell effector functions. *Proc. Natl Acad. Sci. USA* **110,** E2480–E2489 (2013).
26. Miyazaki, A., Yogosawa, S., Murakami, A. & Kitamura, D. Identification of CMTM7 as a transmembrane linker of BLNK and the B-cell receptor. *PLoS ONE* **7,** e31829 (2012).
27. Benjamini, Y. & Hochberg, Y. Controlling the False discovery rate: a practical and powerful approach to multiple testing. *J. R. Stat. Soc. B* **57,** 289–300 (1995).

Supplementary Information is available in the online version of the paper.

Acknowledgements We thank F. Scheeren, E. Stickel, V. Blomen, M. Brockmann and the other members of the Schumacher and Brummelkamp laboratories for discussions, J. Grabowska for technical assistance, K. Kemper and D. Peeper for sharing melanoma PDX models and the NKI- AVL flow facility, the NKI-AVL Core Facility Molecular Pathology & Biobanking (CFMPB) for supplying NKI-AVL Biobank material and/or laboratory support. This work was supported by The Queen Wilhelmina Cancer Research Award and European Research Council (ERC) Advanced Grant SENSIT (to T.N.M.S.), NWO Vici Grant (016.Vici.170.033), the Cancer Genomics Center (CGC.nl), and Ammodo KNAW Award 2015 for Biomedical Sciences (to T.R.B.), The Cancer Research Institute (CRI) Irvington Postdoctoral Fellowship (to C.S.), The Landsteiner Foundation for Blood Research, grant 1355 (to J.B.), Proteins@Work, a program of the Netherlands Proteomics Centre financed by NWO, the Netherlands Organisation for Scientific Research (to A.J.R.H.) and The Institute for Chemical Immunology, an NWO Gravitation project (to T.N.M.S. and A.J.R.H.).

Author Contributions R.M., C.S. and L.T.J. conceived the project, designed and performed experiments, interpreted data and co-wrote the paper. R.G.-E. designed, performed and interpreted functional assays. W.W. designed, performed and interpreted mass spectrometry analyses, A.J.R.H. designed and interpreted mass spectrometry analyses, E.d.V. designed, performed and interpreted immunoprecipitation experiments, Y.X. designed, performed and interpreted human dendritic cell experiments, M.E.W.L. performed and interpreted melanoma PDX experiments, M.S. performed bioinformatic analyses, L.F.A.W. supervised bioinformatic analysis, E.A.R. and I.H. identified samples and performed immunohistochemistry analyses, A.B. and H.M.H. supervised and scored immunohistochemistry analyses, C.U.B. provided and identified samples for immunohistochemistry analyses, J.B. designed and interpreted immunoprecipitation and human dendritic cell experiments, T.R.B. and T.N.M.S. designed experiments, interpreted data and co-wrote the manuscript.

Author Information Reprints and permissions information is available at www.nature.com/reprints. The authors declare competing financial interests: details are available in the online version of the paper. Readers are welcome to comment on the online version of the paper. Publisher's note: Springer Nature remains neutral with regard to jurisdictional claims in published maps and institutional affiliations. Correspondence and requests for materials should be addressed to T.R.B. (t.brummelkamp@nki.nl) or T.N.M.S. (t.schumacher@nki.nl).

Reviewer Information *Nature* thanks S. Ogawa, A. Ribas and the other anonymous reviewer(s) for their contribution to the peer review of this work.

METHODS

Data reporting. No statistical methods were used to predetermine sample size. The experiments were not randomized and the investigators were not blinded to allocation during experiments and outcome assessment.

Cell lines. A375, DLD1, RKO, H2030 and H2122 cells were purchased from the American Type Culture Collection (ATCC). 8505C was purchased from the Deutsche Sammlung von Mikroorganismen und Zellkulturen GmbH (DSMZ). WM2664 and COLO679 cells were gifts from R. Bernards (The Netherlands Cancer Institute). Short-term cell lines from patient-derived melanoma xenografts were generated as described[28] and were a gift from D. Peeper and K. Kemper. HAP1 cells have been described previously[19]. HAP1 cells were cultured in IMDM (Thermo Fisher Scientific) supplemented with 10% fetal calf serum (FCS, Sigma-Aldrich), 100 U ml^{-1} penicillin–streptomycin (Thermo Fisher Scientific) and L-glutamine (Thermo Fisher Scientific); A375 and short-term melanoma xenograft cultures were maintained in DMEM supplemented with 10% FCS (Sigma-Aldrich) and 100 U ml^{-1} penicillin–streptomycin (Thermo Fisher Scientific). All other cell lines were cultured in RPMI supplemented with 10% FCS (Sigma-Aldrich) and 100 U ml^{-1} penicillin–streptomycin (Thermo Fisher Scientific). IFNγ treatment was performed over a period of 48 h at a concentration of 25 ng ml^{-1}, unless indicated otherwise.

Identification of genetic regulators. The approach described in ref. 20 was followed to identify regulators of PD-L1 abundance. Mutagenized HAP1 libraries (starting with either wild-type cells or CMTM6-deficient HAP1 cells) were expanded to approximately 1.5×10^9 cells and subsequently treated with 0.5 ng ml^{-1} IFNγ (Peprotech) for 24 h to induce expression of PD-L1. Subsequently, approximately 3×10^9 cells were dissociated using trypsin-EDTA (Life Technologies), washed with PBS and stained with FITC-labelled anti-PD-L1 antibody (BD Pharmingen) at 1:20 dilution for 30 min at room temperature in PBS containing 0.5% w/v bovine serum albumin (Sigma-Aldrich) and 0.2% w/v sodium azide (Sigma-Aldrich). Subsequently, cells were washed three times with PBS containing 1% FCS and stained with FITC-labelled polyclonal goat anti-mouse Ig (BD pharmingen) at 1:100 dilution for 30 min at room temperature in PBS containing 0.5% w/v bovine serum albumin (Sigma-Aldrich) and 0.2% w/v sodium azide (Sigma-Aldrich) to allow signal amplification. Following two washes with PBS containing 1% FCS and one wash with PBS, stained cells were passed through a 40-μm strainer (BD FalconTM) and subsequently fixed using BD fix buffer I (BD biosciences) for 10 min at 37 °C, followed by a wash with PBS containing 1% FCS. Subsequently, cells were permeabilized by suspension in cold BD permeabilization buffer (BD Biosciences) while vortexing, and incubated on ice for 30 min before incubation with 100 μg ml^{-1} RNase A (Qiagen) and 10 μg ml^{-1} propidium iodide (Cayman Chemical) at 37 °C temperature for 30 min. Alternatively, cells were subjected to treatment with 3 μM 4′,6-diamidino-2-phenylindole (DAPI) for 30 min. Staining of the cells finished with a final wash in PBS containing 10% FCS. Following staining, cells were sorted on a Biorad S3 Cell sorter (Biorad) or a Moflo Asterios cell sorter (Beckman Coulter) to collect the 1–5% of cells with the highest and lowest PD-L1 staining intensity and 1*n* DNA content. Sorted cells were used for isolation of genomic DNA and retroviral gene-trap insertion sites were retrieved, mapped and analysed as described in ref. 20. For PD-L1, it has been described that alterations of the 3′ portion of the gene can stabilize the gene product and lead to higher PD-L1 proteins levels[11]. As this was also recapitulated by our gene-trap insertion method (gene-trap integrations into the 3′ portion of the gene resulted in increased rather than decreased staining intensity for PD-L1), integrations in the portion of the gene downstream of exon 5 (Refseq identifier NM_014143.3) were disregarded where indicated.

Generation of knockout cell lines. Knockout cell lines were generated using the CRISPR–Cas9 system. To generate knockout HAP1 cells, cells were transfected with a px330 vector (Addgene 42230) encoding a sgRNA for the gene of interest and a vector encoding a sgRNA for the zebrafish TIA gene (5′-GGTATGTCGGGAACCTCTCC-3′), as well as a P2A-blasticidin-resistance cassette flanked by two TIA target sites. This allows incorporation of the blasticidin-resistance gene into the locus of interest, resulting in a stable knockout, essentially as described[29]. Following blasticidin selection (10 μg ml^{-1}), resistant clones were expanded.

To generate knockout A375 and 8505C cells, cells were transfected with pLentiCRISPR v.2 vector (Addgene 52961) encoding sgRNAs targeting non-overlapping regions of the *CMTM6* gene[30]. Following puromycin selection (2 μg ml^{-1}, for two days), single-cell clones were expanded and gene disruptions were validated by sequencing and western blot analysis.

The sgRNA sequence CCGGGTCCTCCTCCGTAGTG was used to generate the A375 CMTM6-knockout clone CMTM6 KO6, the 8505C CMTM6-knockout clone CMTM6 KO1 and the RKO CMTM6-knockout clone, the sgRNA sequence TCACAATGTACTTTATGTGG was used to generate the A375 CMTM6-knockout clone CMTM6 KO12 and the 8505C CMTM6-knockout clone CMTM6 KO3. The sgRNA sequence ACTGCTTGTCCAGATGACTT was used to generate the A375 PD-L1-knockout clone and the sgRNA sequence GGAGATGGAGAGCTATGATG was used to generate all the *STUB1*-knockout clones.

Immunoprecipitation, SDS–PAGE and western blot analysis. Cells for western blot analysis were seeded in six-well plates and cultured as described in the figure legends. To collect cell lysates, cells were washed with PBS and lysed with RIPA buffer supplemented with freshly added protease inhibitor cocktail (Roche). After incubation on ice for 30 min, cell lysates were centrifuged at 20,000*g* for 15 min at 4 °C. Supernatants were subsequently processed using a Novex NuPAGE Gel Electrophoresis System, according to the manufacturer's instructions (Thermo Fisher Scientific).

Cells for (co)immunoprecipitation experiments were seeded in 15-cm dishes and cultured as described in the figure legends, using 5 million cells per immunoprecipitation reaction. Cells were washed with cold PBS buffer and lysed in CHAPS buffer (1% CHAPS, 50 mM Tris-HCl pH 7.5, 150 mM NaCl). For the detection of protein ubiquitination, cells were lysed in denaturing buffer (50 mM Tris-HCl, 0.5 mM EDTA and 1% SDS) followed by heating at 95 °C for 10 min and then quenched by adding nine volumes of quenching buffer (0.5% Triton X-100, 20 mM Tris-HCl (pH 8.0), 137 mM NaCl, 10% glycerol, 2 mM EDTA). Protease inhibitor cocktail (Roche) was freshly added to all buffers. Cell lysates were incubated on a rotator for 30 min at 4 °C, and then centrifuged at 20,000*g* for 15 min at 4 °C. Supernatants were subsequently processed using Dynabeads Protein A or Protein G for Immunoprecipitation (Thermo Fisher Scientific), and the indicated antibodies. The final elute was processed and western blot analysis was performed using a Novex NuPAGE Gel Electrophoresis System, according to the manufacturer's instructions (Thermo Fisher Scientific).

Pulse–chase and EndoH or PNGaseF treatment. V5-tagged PD-L1-transduced CMTM6-overexpressing A375 cells and V5-tagged PD-L1-transduced CMTM6-knockout A375 cells were cultured in methionine- and cysteine-free medium for 1 h at 37 °C. Cells were then pulse labelled with 0.5 mCi ml^{-1} [^{35}S]Cys/[^{35}S]Met (PerkinElmer) for 1 h. Cells were washed with PBS to remove residual [^{35}S]Cys/[^{35}S]Met and then cultured in regular medium with extra 'cold' methionine and cysteine for 0, 1, 2, 3 and 6 h. Cell samples were lysed and used for immunoprecipitation with anti-V5 antibody (Thermo Fisher Scientific) immobilized on protein-A- or protein-G-coated beads (Thermo Fisher Scientific). Immunoprecipitates were either left untreated or treated with EndoH or PNGaseF (New England Biolabs), according to the manufacturer's instructions.

Immunoprecipitates were run on NuPAGE 4–12% gels. Gels were treated with 1 M Na salicylate pH 5.6 before drying, and then analysed on Fujifilm BAS-MP phosphor imager screens. Quantification was performed using a Fujifilm FLA-3000 phosphor imager and AIDA image analyser software. Gels were exposed to film using intensifier screens at −80 °C.

Viral vectors. Lentiviral shRNA vectors were retrieved from the arrayed TRC human genome-wide shRNA collection. Additional information is available at http://www.broadinstitute.org/rnai/public/clone/search using the TRCN number. The following lentiviral shRNA vectors were used: shCMTM6-4: TRCN0000127888; shCMTM6-6: TRCN0000130177; shCMTM4-1: TRCN0000142717; shCMTM4-2: TRCN0000142470.

PD-L1, PD-1, PD-L2, CMTM6, CMTM4 and PD-L1–PD-L2 chimaeras expressing lentiviral vectors were generating by insertion of the relevant gBlock (IDT) into a pCDH-CMV-MCS-EF1-Puro (CD510B-1, System Bioscience)-derived vector in which the puromycin-resistance cassette was substituted with a blasticidin-resistance cassette. PD-L1–PD-L2 chimaeras were generated as follows. Each section in brackets is a separate unit of amino acids (a.a.) from PD-L1 or PD-L2 or the sequence of the Flag-epitope tag (DYDDDDKD): PD-L1–PD-L2 TM (transmembrane): (a.a. 1–18 PD-L1)–(DYDDDDKD)–(a.a. 19–238 PD-L1)–(a.a. 221–242 PD-L2)–(a.a. 263–290 PD-L1). PD-L1–PD-L2 IC (intracellular): (a.a. 1–18 PD-L1)–(DYDDDDKD)–(a.a. 19–262 PD-L1)–(a.a. 246–273 PD-L2). PD-L1–PD-L2 EC (extracellular): (a.a. 1–20 PD-L2)–(DYDDDDKD)–(a.a. 21–221 PD-L2)–(a.a. 232–290 PD-L1). For the generation of chimaeras, isoforms NP_054862.1 (PD-L1) and NP_079515.2 (PD-L2) were used.

V5-tagged PD-L1 was retrieved from the CCSB-Broad Lentiviral Expression Library (ccsbBroad304_15876). CMTM family members were ordered as individual gBlocks (IDT) coding for the different family members using Ensembl gold transcripts ENST00000379500.6 (CMTM1), ENST00000268595.2 (CMTM2), ENST00000361909.8 (CMTM3), ENST00000330687.8 (CMTM4), ENST00000339180.8 (CMTM5), ENST00000205636.3 (CMTM6), ENST00000334983.9 (CMTM7), ENST00000307526.3 (CMTM8) C-terminally fused with a Flag tag, preceded by a short AAV-linker and cloned into the pMX-IRES-Blast vector using restriction enzymes BglII and SalI (CMTM1 and

CMTM4), EcoRI and NotI (CMTM2) or BamHI and SalI (CMTM3, CMTM5, CMTM6, CMTM7 and CMTM8). The retroviral vector pBABE-Puro encoding C-terminally Flag-tagged CMTM6 (pBp-CMTM6-Flag) was generated by cloning a gBlock for CMTM6 (ENST00000205636.3) digested with BamHI and XhoI into pBABE-Puro digested with BamHI and SalI.

For production of lentiviral particles, the described plasmids were co-transfected into HEK293T cells along with packaging plasmids (pPAX2, pVSV-G). Two days after transfection, lentiviral supernatant was collected and used for transduction. Retroviral particles were produced and purified as described for HAP1 mutagenesis, except that multiple collections and ultracentrifugation were omitted. Two days after transduction, cells were selected by exposing them to blasticidin or puromycin.

Antibodies. The following antibodies were used for western blot analyses and immunoprecipitation: anti-HSP90: H114 (SantaCruz); anti-CMTM6: HPA026980 (Atlas) or anti-CMTM6 monoclonal antibody (clone RCT8) directed against a peptide in the C-terminal domain of CMTM6 generated by Absea; anti-CMTM4: HPA014704 (Atlas); anti-PD-L1 for western blot analysis: 405.9A11 (Cell Signaling) or immunoprecipitation: E1L3N (Cell Signaling); normal rabbit IgG: 2729 (Cell Signaling); anti-Flag tag: M2 (Sigma-Aldrich); anti-V5 tag: R960-25 (Thermo Fisher Scientific); anti-STUB1 sc133066 (Santa Cruz); anti-ubiquitin antibody: 3933 (Cell Signaling); goat anti-mouse IgG (H + L)-HRP conjugate (BIO-RAD); and goat anti-rabbit IgG (H + L)-HRP conjugate (BIO-RAD). The following antibodies were used for flow cytometry: anti-PD-L1: M1H1 (eBioscience); anti-PD-L2: 24F.10C12 (Biolegend); anti-MHC-I: BB7.2 (BD bioscience); anti-mouse TCRβ: H57-597 (BD Bioscience); anti-CD8: RPA-T8 (BD bioscience); anti-CD3: SK7 (eBioscience); anti-PD-1: eBioJ105 (eBioscience); anti-IL-2: 554567 (BD Bioscience). The following antibodies were used for immunohistochemistry: anti-PD-L1: 22C3 (DAKO); the anti-CMTM6 monoclonal antibody (clone RCT6) directed against a peptide in the C-terminal domain of CMTM6 was generated by Absea.

RNA isolation, first strand cDNA synthesis and RT–qPCR. Total RNA was isolated from cells using the RNeasy Mini Kit (Qiagen). cDNA was obtained by reverse transcription using the Maxima First Strand cDNA Synthesis Kit for RT–qPCR (Thermo Fisher Scientific), according to the manufacturer's instructions. SensiFAST SYBR No-ROX Kit (Bioline) was used for RT–PCR gene expression analysis, carried out on Roche LightCycler 480 platform. Relative mRNA levels were normalized to *GAPDH* mRNA levels. Primer sets used were as follows: *CD274*-F: ATTTGGAGGATGTGCCAGAG; *CD274*-R: CCAGCACACTGAGAATCAACA; *GAPDH*-F: AAGGTGAAGGTCGGAGTCAA; *GAPDH*-R: AATGAAGGGG TCATTGATGG.

IL-2 production assay. Human peripheral blood T cells (Sanquin) were activated and transduced with a retroviral vector encoding the MART-I specific 1D3 TCR as described[31] and with a lentiviral vector encoding PD-1. MART-I TCR and PD-1 expression was validated by flow cytometry. Both 8505C (parental and CMTM6-KO) and A375 cells (parental, PD-L1-overexpressing, and CMTM6-KO PD-L1-overexpressing) were pulsed with 10 ng ml^{-1} MART-I(26–35) peptide for 1 h at 37 °C. Next, 1×10^5 transduced T cells were incubated with 1×10^5 peptide-pulsed tumour cells or non-pulsed tumour cells in the presence of 1 μl ml^{-1} Golgiplug (BD Biosciences). After a 5-h incubation at 37 °C, cells were washed and stained with phycoerythrin (PE)-labelled anti-mouse TCRβ chain, V500-labelled anti-CD8, PerCP Cy5.5-labelled anti-CD3 and PE Cy7-labelled anti-PD-1 and analysed for IL-2 production by intracellular cytokine staining. Activity of T cells with different levels of PD-1 expression was analysed by gating on mouse TCRβ-chain-positive cells expressing low, intermediate or high levels of PD-1.

Membrane fractionation and MS analysis. Snap-frozen cell pellets were lysed by gentle homogenization in isotonic buffers supplemented with phosphatase inhibitor (PhosSTOP, Roche) and protease inhibitor (cOmplete mini EDTA-free, Roche). Cellular disruption of >95% was confirmed by microscopy. Plasma membrane (F4), inner membrane (F3) and cytosolic (F1) fractions were prepared by differential centrifugation using a plasma membrane purification kit (Abcam, ab65400).

From fractions F1, F3 and F4, 20 μg of protein was diluted 20 times in 50 mM ammonium bicarbonate, reduced in 4 mM dithiothreitol (DTT), alkylated in 8 mM iodoacetamide (IAA) and digested sequentially at 37 °C with 1:75 Lys C (Wako) and 1:50 trypsin (Sigma-Aldrich) for 4 and 12 h, respectively. Digested peptides were acidified to 0.1% formic acid (FA) and purified by strong cation exchange (SCX) STAGE tips, using as loading buffer: 80% acetonitrile (ACN), 0.1% FA and as elution buffer: 0.5 M ammonium acetate, 20% ACN, 0.1% FA. Eluted peptides were dried by vacuum and 4 μg equivalent of peptides was analysed in a 3 h reverse-phase separation on the UHPLC 1290 system (Agilent) coupled to an Orbitrap Q Exactive HF mass spectrometer (Thermo Fisher Scientific). SCX flowthrough from cytosolic fraction (denoted F2) was analysed separately to increase proteome coverage.

RP-nanoLC–MS/MS. Proteomics data were acquired using an UHPLC 1290 system (Agilent) coupled to an Orbitrap Q Exactive HF spectrometer (Thermo Scientific). Peptides were first trapped on a 2 cm × 100 μm Reprosil C18 pre-column (3 μm) and then separated on a 50 cm × 75 μm Poroshell EC-C18 analytical column (2.7 μm). Trapping was performed for 10 min in 0.1 M acetic acid (solvent A) and elution with 80% ACN in 0.1 M acetic acid (solvent B) in gradients as follows: 10–40% solvent B in 155 min, 40–100% in 3 min and finally 100% for 1 min. Flow was passively split to 300 nl min^{-1}. MS data were obtained in data-dependent acquisition mode. Full scans were acquired in the m/z range of 375–1,600 at the resolution of 35,000 (m/z 400) with AGC target 3×10^6. The top 15 most intense precursor ions were selected for HCD fragmentation performed at normalized collision energy (NCE) 25%, after accumulation to target value of 5×10^4. MS/MS acquisition was performed at a resolution of 17,500.

Database search. Raw files were processed using MaxQuant version 1.5.3.30 and searched against the human Swissprot database (version May 2016) using Andromeda.

Cysteine carbamidomethylation was set to fixed modification, while variable modifications of methionine oxidation and protein N-terminal acetylation, as well as up to 2 missed cleavages were allowed. The false discovery rate (FDR) was restricted to 1% in both protein and peptide identification. Label-free quantification (LFQ) was performed with 'match between runs' enabled.

Analysis of *CMTM6* RNA levels and correlation between *CMTM6* and *CD274* RNA levels in TCGA samples. TCGA RNA sequencing data were downloaded from the Broad TCGA genome data analysis centre 1 November 2015 release of the standard runs (http://gdac.broadinstitute.org/runs/stddata). For projects where data from multiple sequencing platforms were available, Illumina HiSeq data was preferentially used. The (RSEM) normalized read count field was multiplied by 10^6 to arrive at the reported TPM expression values. Correlation coefficients and associated unadjusted P values between CMTM6 and CD274 were computed per TCGA-sequencing project with Pearson's method. Two-dimensional kernel density estimates were computed using the MASS::kde2d() function in version 3.3.1 of the R programming language. We computed the correlations between CMTM6 and 10^4 randomly selected genes (identical between sequencing projects) to obtain a reference distribution of correlation coefficients for CMTM6, specific for each TCGA project. The reported empirical P values are defined as one minus the quantile of the CMTM6 and CD274 correlation within this reference distribution.

Immunohistochemistry. Immunohistochemistry of the formalin-fixed paraffin-embedded samples was performed on a BenchMark Ultra autostainer (Ventana Medical Systems). In brief, 3 μm paraffin serial sections were cut, heated at 75 °C for 28 min and deparaffinized in the instrument with EZ prep solution (Ventana Medical Systems). Heat-induced antigen retrieval was carried out using Cell Conditioning 1 (CC1, Ventana Medical Systems) for 48 min for PD-L1 and 64 min for CMTM6 antibodies at 95 °C.

PD-L1 clone 22C3 (DAKO) was used at 1:40 dilution, 1 h at room temperature and CMTM6 clone RCT6 was used directly from hybridoma supernatant at either 1:500 or 1:1,000 dilution for tumour samples and 1:100 dilution for cell lines, 1 h at room temperature. Bound antibody was detected using the OptiView DAB Detection Kit (Ventana Medical Systems). Slides were counterstained with Haematoxylin and Bluing Reagent (Ventana Medical Systems).

Patient melanoma samples were obtained (following Institutional Review Board approval) from the NKI-AVL pathology archive biobank and selected for PD-L1 expression.

Statistical analysis. All student t-tests were two-tailed under the assumption of equal variance between samples.

Data availability. All sequencing datasets have been deposited in the NCBI Sequence Read Archive under accession number SRP108407. In addition, all processed screen results are accessible in an interactive database (https://phenosaurus.nki.nl/). Source Data for the main and extended data figures are provided in the online version of the paper.

28. Kemper, K. *et al.* Intra- and inter-tumor heterogeneity in a vemurafenib-resistant melanoma patient and derived xenografts. *EMBO Mol. Med.* **7,** 1104–1118 (2015).
29. Lackner, D. H. *et al.* A generic strategy for CRISPR–Cas9-mediated gene tagging. *Nat. Commun.* **6,** 10237 (2015).
30. Doench, J. G. *et al.* Optimized sgRNA design to maximize activity and minimize off-target effects of CRISPR–Cas9. *Nat. Biotechnol.* **34,** 184–191 (2016).
31. Jorritsma, A. *et al.* Selecting highly affine and well-expressed TCRs for gene therapy of melanoma. *Blood* **110,** 3564–3572 (2007).

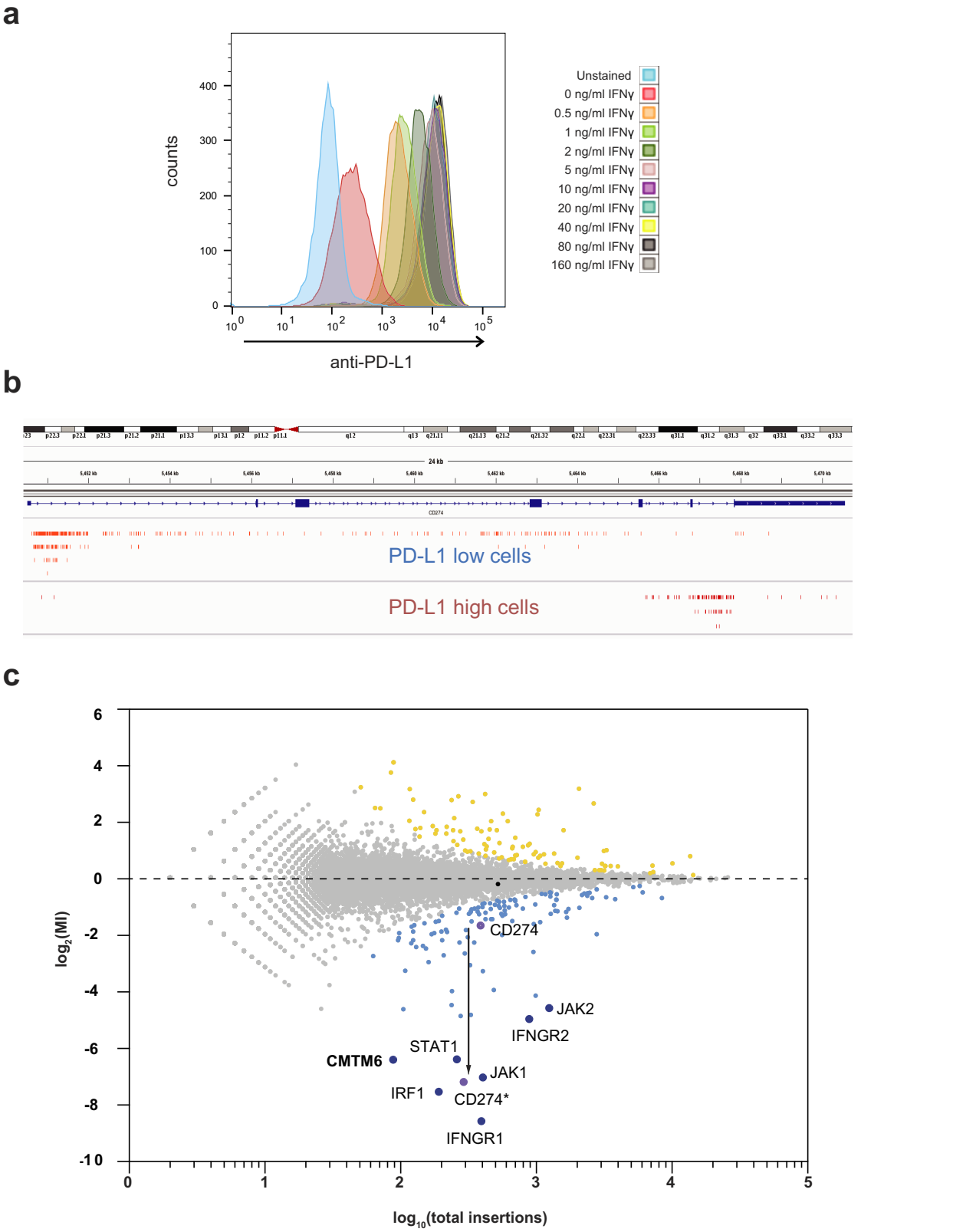

Extended Data Figure 1 | PD-L1 is regulated by IFNγ and by the 3′ UTR in HAP1 cells. a, Flow cytometry analysis of PD-L1 expression in untreated HAP1 cells and HAP1 cells treated with the indicated concentrations of IFNγ. An IFNγ concentration of 0.5 ng ml^{-1} was chosen for the subsequent genetic screen, to allow identification of gene integrations that either enhance or suppress PD-L1 expression. Data are representative of three independent experiments. **b**, Schematic representation of the PD-L1 gene and of the gene trap insertions observed in HAP1 cells sorted on the basis of either low or high PD-L1 expression. Note the bias towards integrations within introns 5 and 6 in the *PD-L1* gene in PD-L1^{high} cells relative to PD-L1^{low} cells, consistent with the structural variants beyond exon 4 of *PD-L1* that have been shown to result in increased PD-L1 expression in a subset of adult T-cell leukaemia, diffuse large B-cell lymphoma and stomach cancers[11]. **c**, Screen data as depicted in Fig. 1, but now with PD-L1 (*CD274*) data plotted when either including (*CD274*) or excluding (*CD274**) integrations downstream of exon 5 (Refseq identifier NM_014143.3). MI, mutation index.

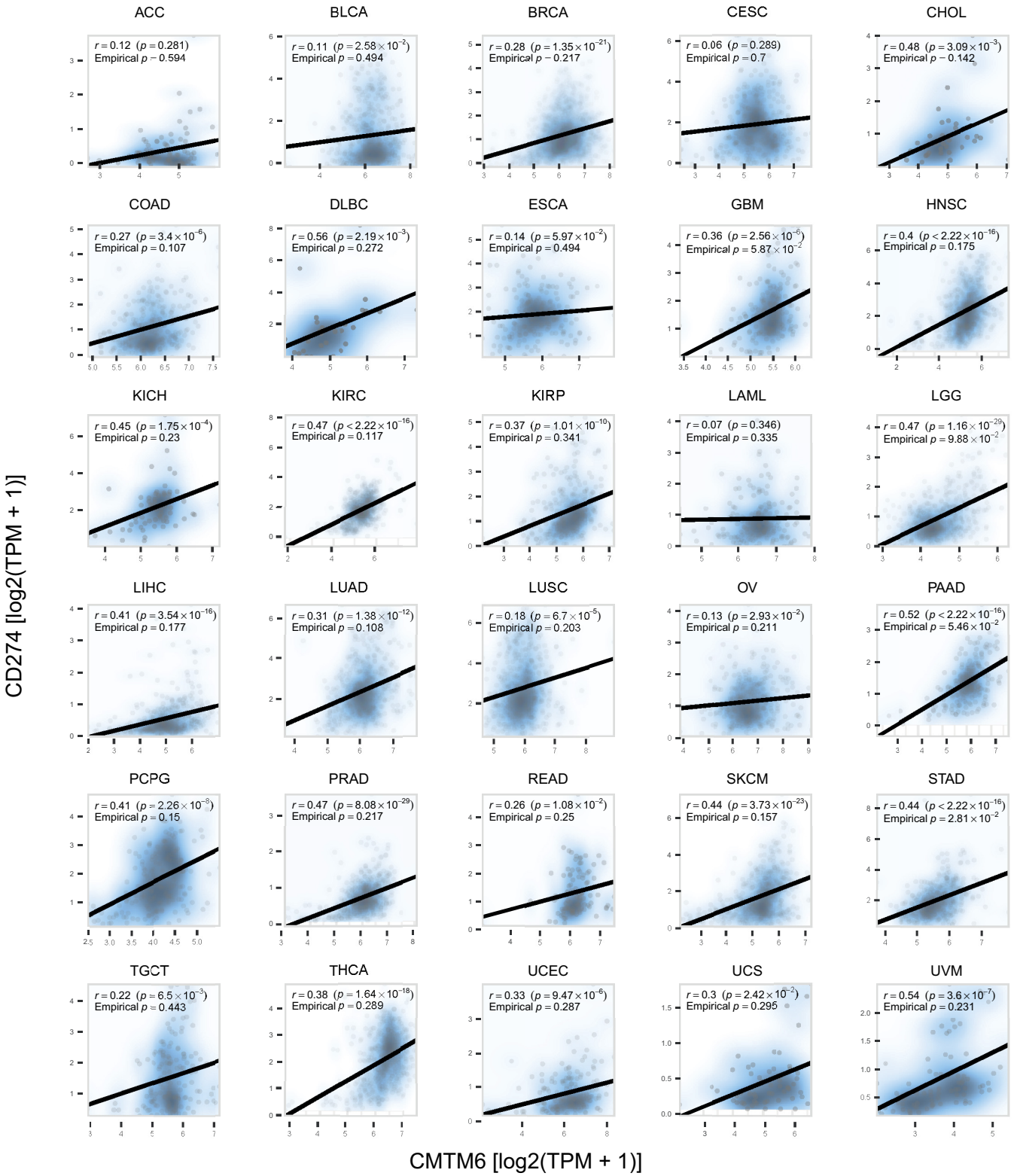

Extended Data Figure 2 | See next page for caption.

Extended Data Figure 2 | RNA expression of *CMTM6* in human cancers and correlation with *PD-L1* mRNA levels. Pearson's correlation coefficients (*r*) are shown along with associated unadjusted *P* values. Because randomly selected genes are on average also weakly positively correlated (not shown), empirical *P* values, which represent one minus the quantile of the *CMTM6*- and *CD274*-expression correlation coefficient among a reference distribution composed of correlation coefficients between *CMTM6* and randomly selected genes, are also depicted. Empirical *P* values smaller than 0.5 denote a stronger correlation between *CMTM6* and *CD274* than the median observed correlation in the reference distribution. TPM, transcript per million. ACC, adrenocortical carcinoma; BLCA, urothelial bladder carcinoma; BRCA, breast cancer; CESC, cervical squamous cell carcinoma; CHOL, cholangiocarcinoma; COAD, colorectal adenocarcinoma; DLBC, diffuse large B-cell lymphoma; ESCA, oesophageal cancer; GBM, glioblastoma multiforme; HNSC, head and neck squamous cancer; KICH, chromophobe renal cell carcinoma; KIRC, clear cell kidney carcinoma; KIRP, papillary kidney carcinoma; LAML, acute myeloid leukaemia; LGG, lower grade glioma; LIHC, liver hepatocellular carcinoma; LUAD, lung adenocarcinoma; LUSC, lung squamous cell carcinoma; OV, ovarian serous cystadenocarcinoma; PAAD, pancreatic ductal adenocarcinoma; PCPG, pheochromocytoma and paraganglioma; PRAD, prostate adenocarcinoma; READ, rectum adenocarcinoma; SKCM, cutaneous melanoma;, STAD, stomach cancer; TGCT, testicular germ cell cancer; THCA, papillary thyroid carcinoma; UCEC, uterine corpus endometrial carcinoma; UCS, uterine carcinosarcoma; UVM, uveal melanoma.

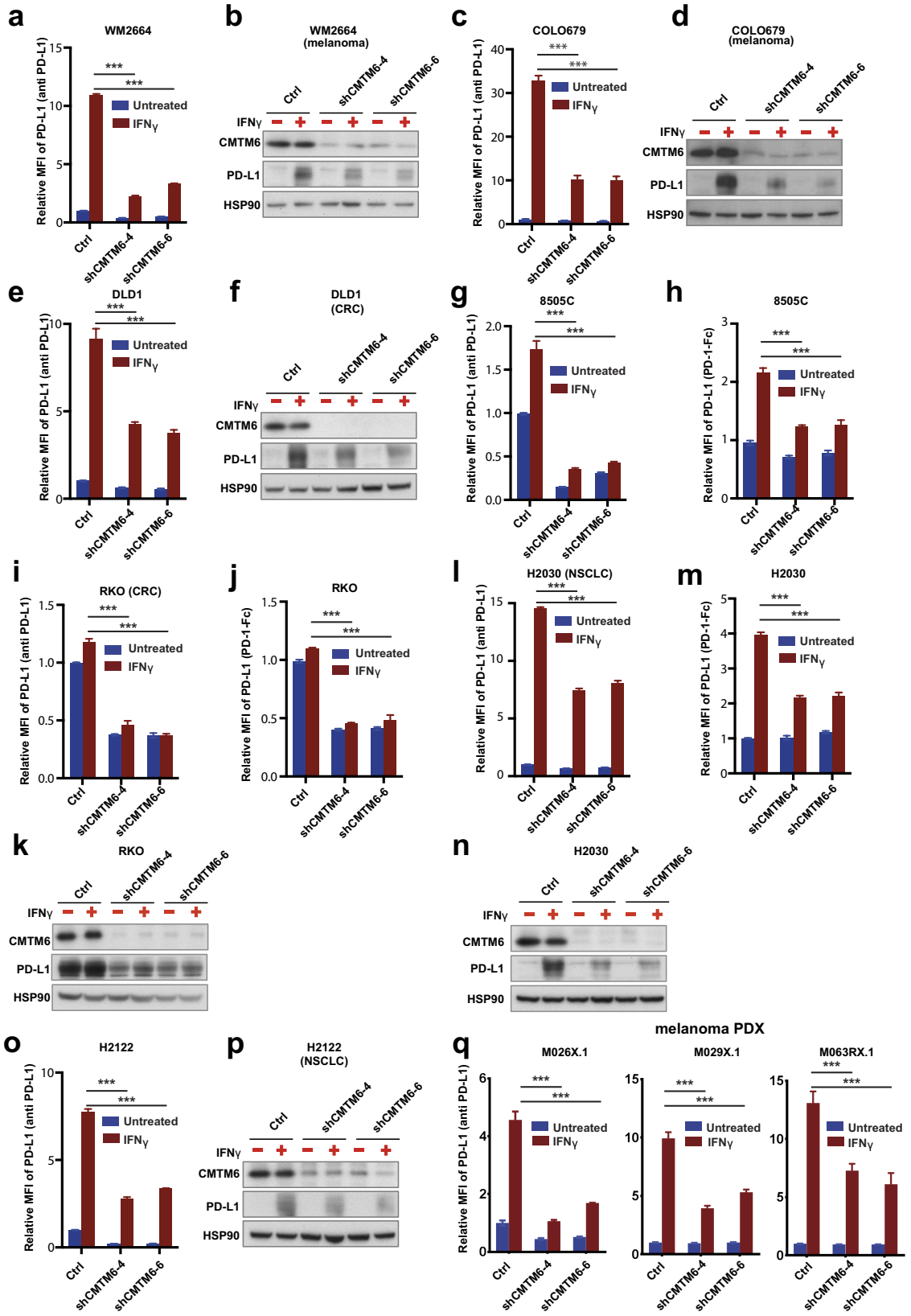

Extended Data Figure 3 | See next page for caption.

Extended Data Figure 3 | Regulation of PD-L1 by CMTM6 in different tumour types. a, **c**, **e**, **o**, **q**, Flow cytometry analysis of PD-L1 expression in WM2664 melanoma cells (**a**), COLO679 melanoma cells (**c**), DLD1 colorectal cancer cells (**e**), H2122 non-small-cell lung cancer cells (**o**) and three short-term cultures of melanoma xenografts (**q**). Cells are independently transduced with two vectors expressing different *CMTM6* shRNAs and are compared with cells transduced with the control vector. **b**, **d**, **f**, **p**, Western blot analysis of CMTM6 and PD-L1 expression in WM2664 melanoma cells (**b**), COLO679 melanoma cells (**d**), DLD1 colorectal cancer cells (**f**), H2122 non-small-cell lung cancer cells (**p**). Cells are independently transduced with two vectors expressing different *CMTM6* shRNAs and are compared with cells transduced with the control vector. **g**–**j**, **l**, **m**, Flow cytometry analysis of PD-L1 expression upon staining with anti-PD-L1 antibody or with PD-1–Fc in 8505C thyroid cancer cells (**g**, **h**), RKO colorectal cancer cells (**i**, **j**) and H2030 non-small-cell lung cancer cells (**l**, **m**). **k**, **n**, Western blot analysis of CMTM6 and PD-L1 expression in RKO colorectal cancer cells (**k**) and H2030 non-small cell lung cancer cells (**n**). Cells are independently transduced with two vectors expressing different *CMTM6* shRNAs and are compared with cells transduced with the control vector. In all cases, cells treated with IFNγ (25 ng ml^{-1}) or left untreated were compared. **g**, The graph shown is identical to Fig. 2f, shown again here to facilitate comparison. Data are representative of three (**c**–**n**), two (**a**, **b**, **o**, **p**) or one (**q**) independent experiments and were analysed by unpaired *t*-test (**a**, **c**, **e**, **g**–**m**, **o**, **q**). Data are mean ± s.d. of triplicates (**a**, **c**, **e**, **g**–**m**, **o**, **q**). ***$P < 0.001$. Ctrl, control; MFI, median fluorescence intensity. CRC, colorectal cancer; NSCLC, non-small-cell lung cancer; PDX, patient-derived xenograft.

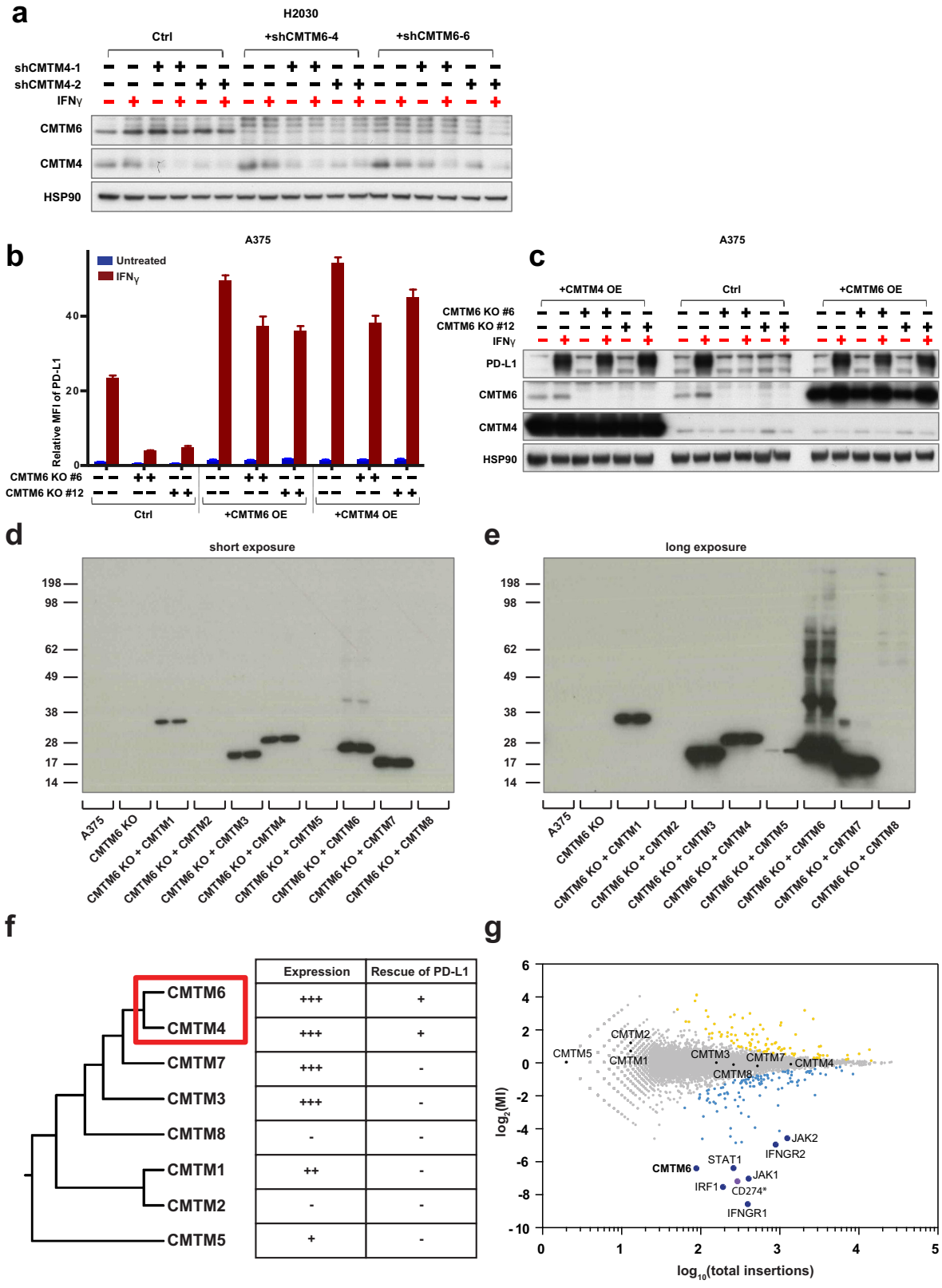

Extended Data Figure 4 | See next page for caption.

Extended Data Figure 4 | CMTM4 and CMTM6, but no other CMTM family members, are regulators of PD-L1. a, Validation of CMTM6 and CMTM4 downregulation by western blot analysis of cells shown in Fig. 3b. **b**, **c**, Ectopic expression of CMTM4 restores IFNγ-induced PD-L1 expression in CMTM6-deficient cells. Two clones of CMTM6-deficient A375 cells (CMTM6 KO #6 and CMTM6 KO #12) were transduced with retroviral vectors encoding CMTM4 (CMTM4 OE) or CMTM6 (CMTM6 OE) individually. After blasticidin selection, cells were cultured in the absence (untreated) or presence of 25 ng ml^{-1} IFNγ for 72 h before flow cytometry (**b**) and western blot (**c**) analysis. Untransduced A375 parental cells served as controls. **d**, **e**, Western blot analysis of expression of the indicated CMTM family members, as determined by staining with an anti-Flag antibody. Two exposures of the same gel are shown. Expression of CMTM2 and CMTM8 is not detected and CMTM5 expression is low compared to that of other CMTM family members. **f**, Phylogenetic analysis of the CMTM family by CLUSTALW. CMTM6 and CMTM4 form the two most closely related members. In view of the lack of detectable expression/low expression observed for CMTM2, CMTM8 and CMTM5, an effect of these CMTM members on PD-L1 protein fate cannot be excluded. However, the observation that CMTM family members 7 and 3, which are more closely related to CMTM4 and CMTM6, do not influence PD-L1 expression makes this unlikely. **g**, Results of the flow-cytometry-based screen as shown in Fig. 1a, with the position of all CMTM family members indicated. Data are representative of two independent experiments (**a**–**e**). Data are mean ± s.d. of triplicates (**b**). KO, knockout; MFI, median fluorescence intensity; MI, mutation index; OE, overexpression.

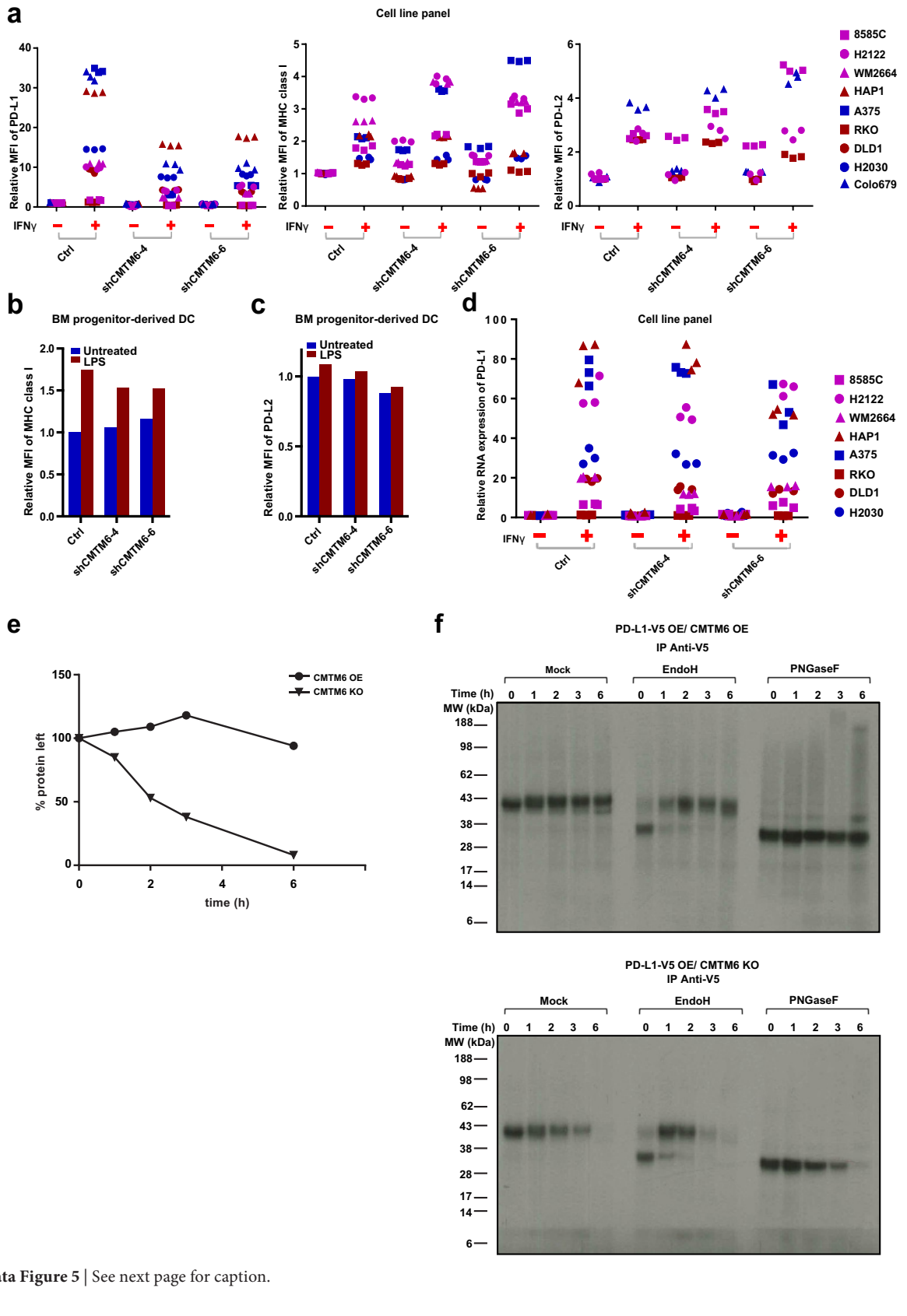

Extended Data Figure 5 | See next page for caption.

Extended Data Figure 5 | CMTM6 downregulation does not affect MHC class I and PD-L2 cell-surface levels or *PD-L1* mRNA levels and regulates PD-L1 stability after egress from the endoplasmic reticulum. **a**–**c**, Flow cytometry analysis of MHC class I and PD-L2 expression in the panel of cell lines tested in Fig. 2 and Extended Data Fig. 3 (**a**), and in bone marrow progenitor-derived dendritic cells (**b**, **c**) in which cells transduced with the control vector are compared with cells independently transduced with two vectors expressing different shRNA directed against *CMTM6*. For cell lines, cells treated with IFNγ (as indicated in the other figure legends) or left untreated were compared, for bone marrow progenitor-derived dendritic cells, cells treated with 500 ng ml^{-1} LPS or left untreated were compared. **d**, qPCR analyses were performed to quantify relative mRNA levels of PD-L1 in the indicated tumour cell lines. **e**, Quantification of the experiment shown in Fig. 4c. **f**, Immunoprecipitates of the samples used in Fig. 4c. Samples were mock-treated, treated with EndoH or with PNGaseF to examine the kinetics of protein maturation. No difference in maturation kinetics was observed between CMTM6-overexpressing and CMTM6-deficient cells. Pulse–chase experiments were performed three times, once comparing CMTM6-overexpressing and CMTM6-deficient cells (**a**) and twice comparing wild-type and CMTM6-deficient cells. Other data are representative of at least two independent experiments. BM, bone marrow; DC, dendritic cell; EndoH, endoglycosidase H; KO, knockout; MFI, median fluorescence intensity; OE, overexpression; PNGaseF, peptide-N-glycosidase F.

a

Cell line	Uniprot accession	Protein name	Gene name	Unique peptides	Mol. weight [kDa]	Sequence length	MS/MS count					Sequence coverage [%]	LFQ intensity
							[F1] Cytosolic	[F2] Cytosolic SCX FT	[F3] Inner memb	[F4] Plasma memb	Total in 4 fractions		
8505c_WT	Q9NX76	CKLF-like MARVEL transmembrane domain-containing protein 6	CMTM6	3	20.419	183	1	2	4	7	14	21.3	6.49E+08
	Q9NZQ7	Programmed cell death 1 ligand 1	CD274	6	33.275	290	10	2	14	38	64	32.1	9.54E+09
RKO_WT	Q9NX76	CKLF-like MARVEL transmembrane domain-containing protein 6	CMTM6	3	20.419	183	1	0	2	6	9	21.3	2.77E+08
	Q9NZQ7	Programmed cell death 1 ligand 1	CD274	6	33.275	290	5	4	20	20	49	32.1	6.70E+09

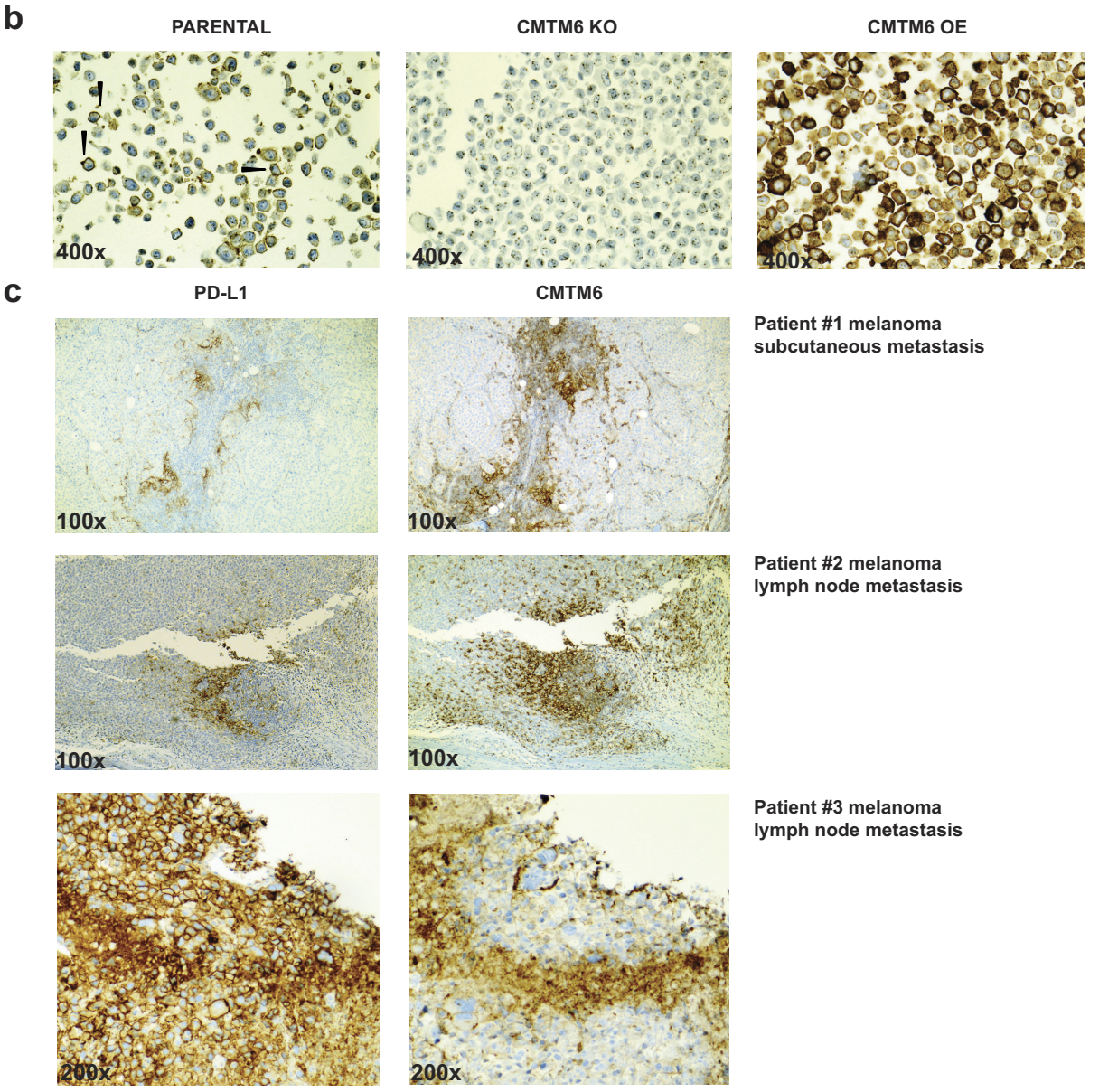

Extended Data Figure 6 | Specificity and membrane localization of CMTM6, and co-localization with PD-L1 in human tumours. **a**, Membrane-fractionated proteome of 8505C and RKO cells. CMTM6 and PD-L1 were detected by LC–MS/MS predominantly from the plasma membrane fractions. Label-free quantification (LFQ) performed by intensity-based normalization of four fractions together across different cell lines is depicted. **b**, A375 parental cells, CMTM6-knockout or CMTM6-overexpressing cells were fixed and formalin embedded, and stained for CMTM6 with a monoclonal antibody (clone RCT6) generated against a peptide from the C-terminal domain of CMTM6. Analysis shows a mainly membranous stain, as indicated by the arrowheads. **c**, Sequential slides from lymph node and subcutaneous metastases from three melanoma patients were stained for PD-L1 (left) or CMTM6 (right), showing frequent localization of PD-L1 within $CMTM6^{+}$ areas. In total, samples from nine melanoma patients and five $PD\text{-}L1^{+}$ lung cancer samples were analysed. KO, knockout; OE, overexpression.

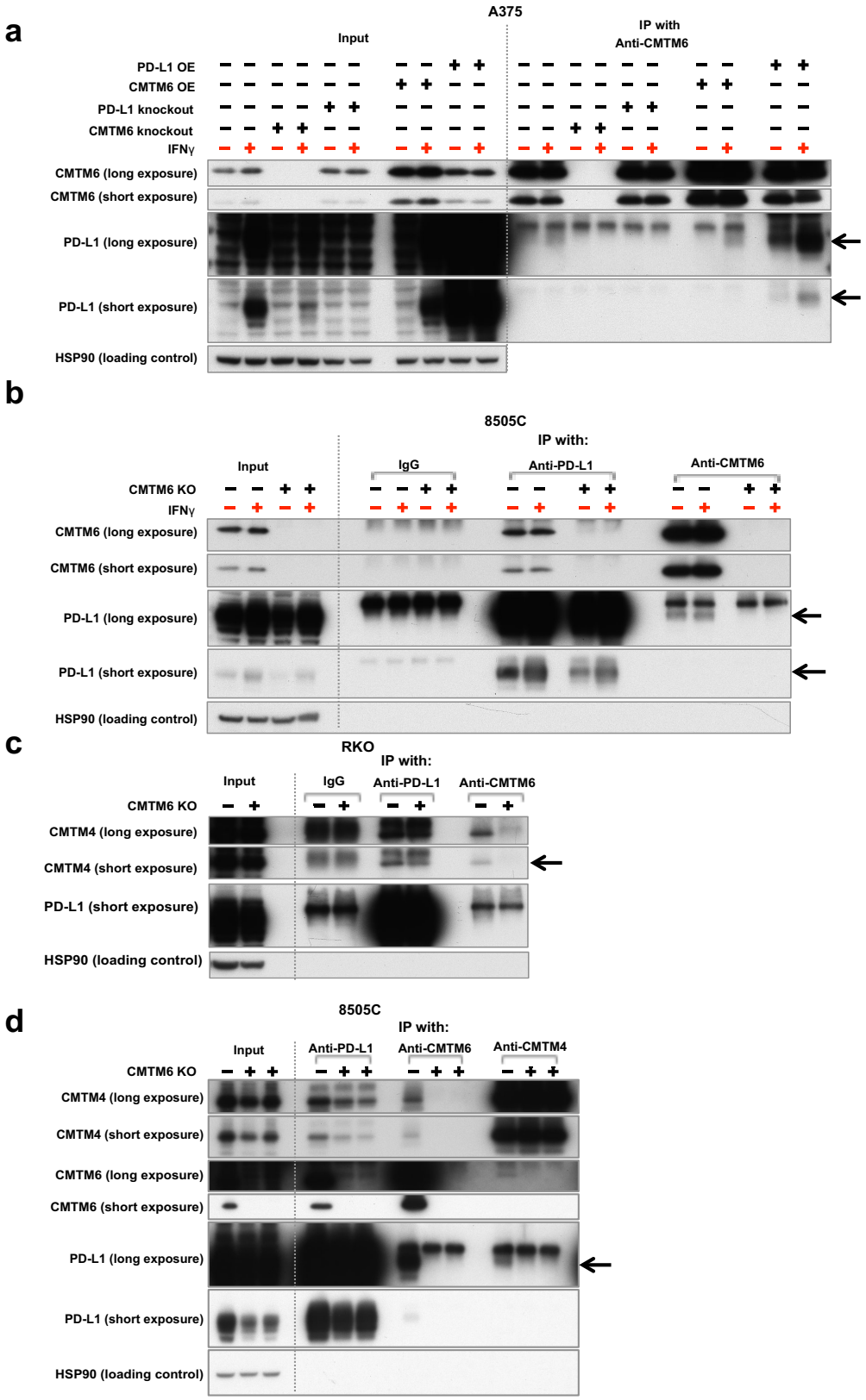

Extended Data Figure 7 | See next page for caption.

Extended Data Figure 7 | Interactions between CMTM6, PD-L1 and CMTM4, and effect of CMTM6 on PD-L1 stability. a, A375 parental cells, CMTM6-deficient cells, PD-L1-deficient cells and cells ectopically expressing CMTM6 or PD-L1, were cultured in the absence or presence of 25 ng ml^{-1} IFNγ for 48 h before preparation of cell lysates. Immunoprecipitation was performed using a CMTM6-specific antibody immobilized on protein-A-coated beads. Immunoprecipitates and whole cell lysate were subjected to SDS–PAGE and immunoblotted for CMTM6 and PD-L1. Two exposures of the same western blot are shown. Arrows indicate PD-L1 bands. **b**, Parental and CMTM6-deficient 8505C cells were cultured in the absence or presence of 50 ng ml^{-1} IFNγ for 72 h before preparation of cell lysates. Immunoprecipitation was performed using CMTM6- or PD-L1-specific antibodies immobilized on protein-A-coated beads. Immunoprecipitates and whole cell lysates were subjected to SDS–PAGE and immunoblotted for CMTM6 and PD-L1. Two exposures of the same western blot are shown. Normal IgG served as a control. Arrows indicate PD-L1 bands. **c**, **d**, Parental and CMTM6-knockout RKO cells (**c**) and 8505C cells (**d**) were lysed and immunoprecipitation was performed using antibodies immobilized on protein-G-coated beads as indicated. Immunoprecipitates and whole-cell lysates were subjected to SDS–PAGE, and western blot analysis of CMTM4 and PD-L1 expession was carried out. Two exposures of the same western blots are shown. Arrows indicate CMTM4 (**c**) or PD-L1 (**d**). Data are representative of three independent experiments. KO, knockout; OE, overexpression.

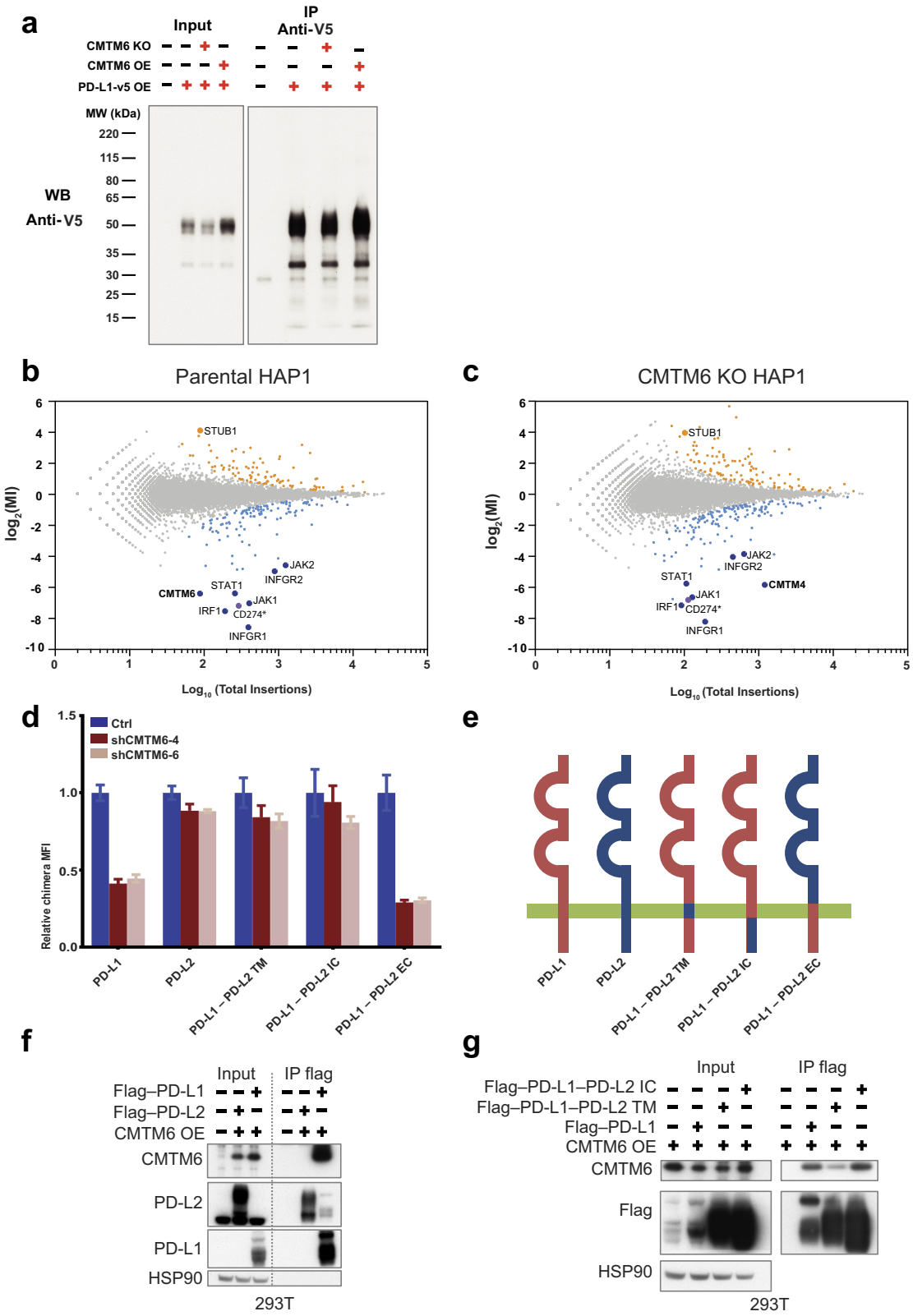

Extended Data Figure 8 | See next page for caption.

Extended Data Figure 8 | Aspects of PD-L1 regulation by CMTM6 and STUB1. a, V5-tagged PD-L1 was introduced into parental, CMTM6-overexpressing and CMTM6-deficient A375 cells. Cell lysates were denatured and then subjected to immunoprecipitation with anti-V5 antibody immobilized on protein-G-coated beads. Immunoprecipitates were then analysed by immunoblotting with an anti-V5 antibody as a control for the experiments shown in Fig. 4e. **b**, **c**, Results of the FACS-based genetic screens in CMTM6-expressing and CMTM6-deficient HAP1 cells as shown in Fig. 1a (**b**) and in Fig. 3a (**c**), with the position of STUB1 indicated. **d**, Relative expression of PD-L1, PD-L2 and the indicated PD-L1–PD-L2 chimaeric proteins in CMTM6 knockdown A375 cells compared to matched control. Chimaeras were detected with an anti-PD-L1 or an anti-PD-L2 antibody. **e**, Schematic overview of the chimaeric proteins analysed. **f**, **g**, HEK293T human embryonic kidney cells were co-transfected with a vector encoding either PD-L1, PD-L2 or the indicated chimaeric protein, together with a vector encoding CMTM6. Cell lysates were denatured and subjected to immunoprecipitation with anti-Flag antibody immobilized on protein-G-coated beads. Lysates and immunoprecipitates were then analysed by immunoblotting with the indicated antibodies. Data are representative of three (**a**, **d**), one (**f**) or two (**g**) independent experiments. Data represent mean ± s.d. of triplicates. EC, extracellular; IC, intracellular; KO, knockout; MFI, median fluorescence intensity; OE, overexpression; TM, transmembrane.

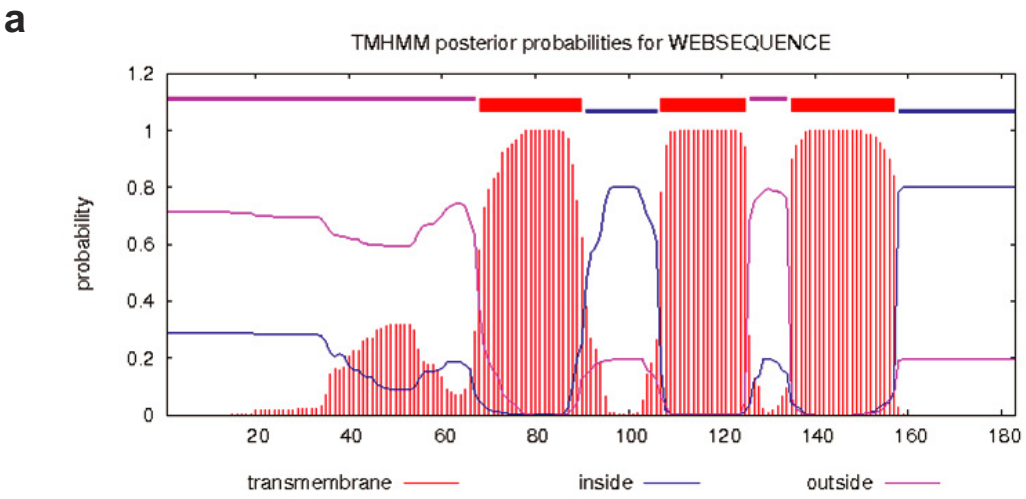

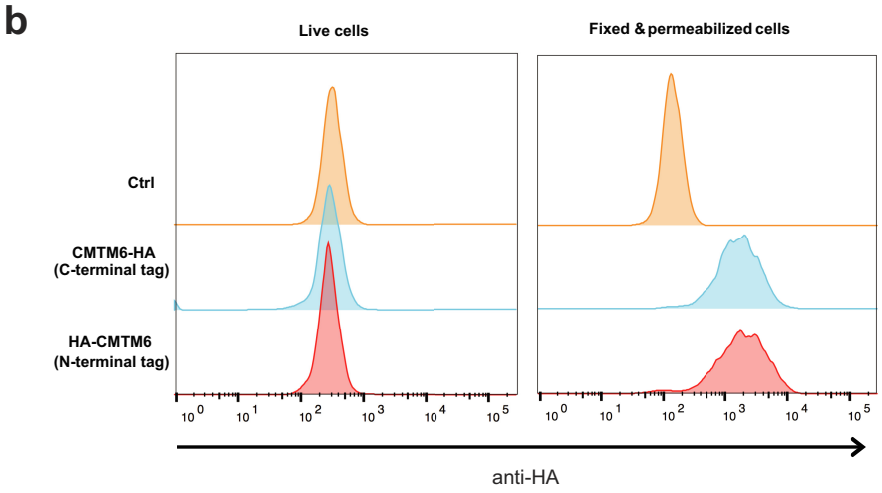

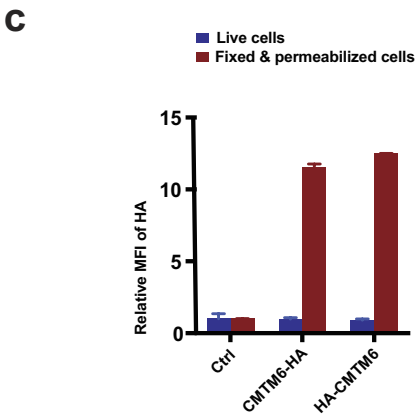

Extended Data Figure 9 | Orientation mapping of CMTM6. a, Predicted domain topology of CMTM6 according to TMHMM Server v. 2.0 (http://www.cbs.dtu.dk/services/TMHMM/). **b**, **c**, A375 cells were transduced with C- or N-terminal haemagglutinin (HA)-epitope-tagged CMTM6. HA-epitope tag staining was performed in both live cells and fixed and permeabilized cells followed by flow cytometry analysis and quantified in **c**. Data represent mean ± s.d. of triplicates. MFI, median fluorescence intensity.

a

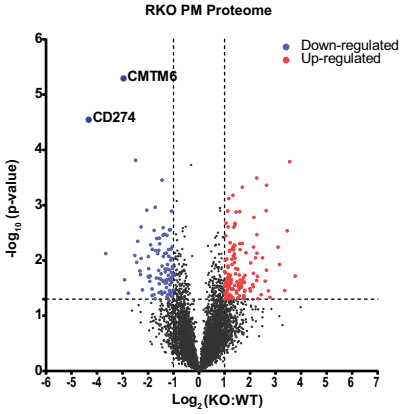

b

No.	Uniprot Accession	Protein name	Gene name	8505 Ave Log2 Intensity [4WT]	8505 Ave Log2 Intensity [4KO]	8505 Fold change [KO:WT]	8505 T.Test p-value [KO:WT]	RKO Ave Log2 Intensity [4WT]	RKO Ave Log2 Intensity [4KO]	RKO Fold change [KO:WT]	RKO T.Test p-value [KO:WT]
1	Q9NZQ7	Programmed cell death 1 ligand 1	CD274	27.05	22.72	0.05	2.84E-05	23.45	28.35	0.03	1.09E-06
2	Q9NX76	CKLF-like MARVEL transmembrane domain-containing protein 6	CMTM6	25.56	22.60	0.13	5.10E-06	22.91	25.35	0.18	2.96E-06
3	A0A024R7X0	Brefeldin A-inhibited guanine nucleotide-exchange protein 1	ARFGEF1	25.74	23.34	0.19	4.50E-03	26.25	27.52	0.41	2.89E-02
4	B5MCA4	Epithelial cell adhesion molecule	EPCAM	23.74	22.64	0.47	6.22E-03	22.92	26.22	0.10	2.91E-03
5	A0A024RDG9	3-hydroxybutyrate dehydrogenase type 2	BDH2	22.62	23.68	2.08	4.27E-02	23.28	22.25	2.04	3.32E-02
6	A0A0G2JN29	Nodal modulator 1	NOMO1	22.94	24.08	2.20	2.47E-03	23.24	21.83	2.66	1.20E-02
7	B4E3Q1	Calsyntenin-1	CLSTN1	22.49	23.65	2.24	7.58E-04	23.64	22.21	2.69	2.16E-02
8	H3BPB8	Mannose-6-phosphate isomerase	MPI	25.32	26.55	2.35	1.85E-02	25.13	22.54	6.02	4.51E-03
9	B3KN28	Phosphoacetylglucosamine mutase	PGM3	24.19	25.44	2.38	4.27E-02	25.18	22.09	8.53	3.26E-04
10	V9HWB7	Aconitate hydratase	HEL60	27.52	28.89	2.58	2.51E-03	24.78	23.20	2.98	4.25E-02
11	X5D2M8	Major vault protein	MVP	28.64	30.90	4.77	3.23E-04	24.11	22.11	3.98	4.12E-02

c

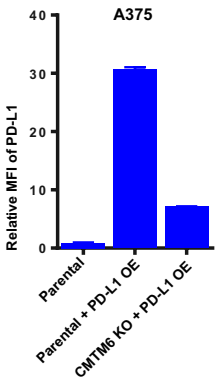

d

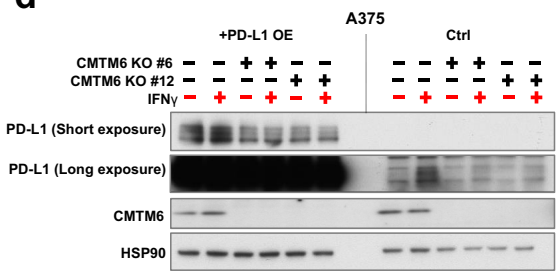

e

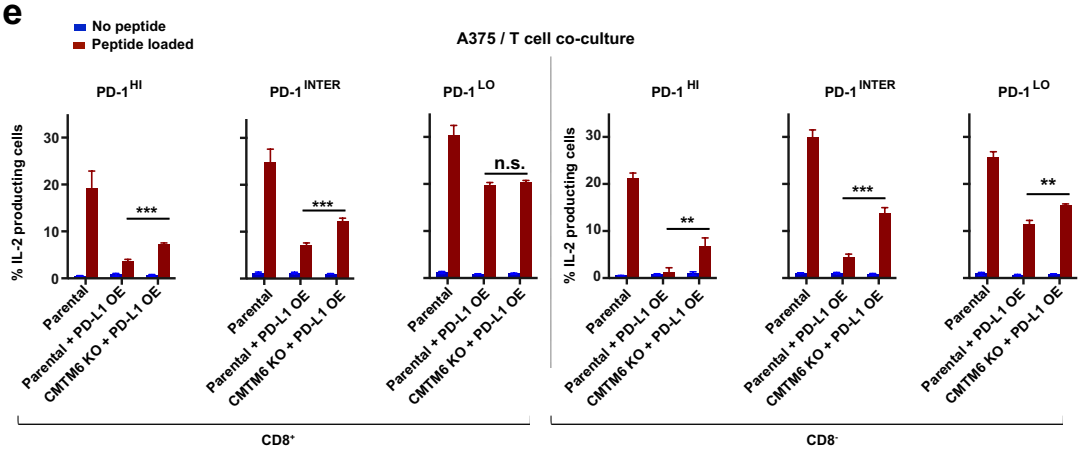

Extended Data Figure 10 | See next page for caption.

Extended Data Figure 10 | Selectivity of CMTM6 and CMTM6 loss alleviates PD-L1-mediated T-cell suppression. a, Comparative membrane-fractionated mass spectrometry of CMTM6-proficient or -deficient RKO cells. Four wild-type and four CMTM6-knockout RKO clones were analysed by LC–MS/MS and differential protein abundance is shown in a volcano plot. **b**, Proteins found up- or downregulated upon CMTM6 removal in both 8505C and RKO cells. **c**, **d**, Flow cytometry (**c**) and western blot (**d**) analysis of CMTM6 and PD-L1 expression in parental A375 or CMTM6-deficient A375 clones in which PD-L1 is ectopically expressed by lentiviral transduction. **e**, Primary human T cells were transduced with the MART-1-specific 1D3 TCR[31] and PD-1. Transduced T cells were co-cultured with unloaded or MART-I peptide-loaded PD-L1-overexpressing A375 cells (Parental + PD-L1 OE), parental A375 cells (Parental) or CMTM6-deficient A375 cells that overexpressed PD-L1 (CMTM6 KO + PD-L1 OE). IL-2 production in T cells that expressed high (PD-1^{high}), intermediate (PD-1^{inter}) or low (PD-1^{low}) levels of PD-1 were analysed by flow cytometry. Untransduced A375 cells (Parental) served as controls. Data are representative of three independent experiments and were analysed by unpaired *t*-test (**c**). Data represent mean ± s.d. of triplicates. $^{**}P < 0.01$; $^{***}P < 0.001$; NS, not significant. KO, knockout; OE, overexpression; PM, plasma membrane; TM, transmembrane; WT, wild type.

nature research

Corresponding Author: Ton Schumacher

Date: Jun 6, 2017

Life Sciences Reporting Summary

Nature Research wishes to improve the reproducibility of the work we publish. This form is published with all life science papers and is intended to promote consistency and transparency in reporting. All life sciences submissions use this form; while some list items might not apply to an individual manuscript, all fields must be completed for clarity.

For further information on the points included in this form, see Reporting Life Sciences Research. For further information on Nature Research policies, including our data availability policy, see Authors & Referees and the Editorial Policy Checklist.

Experimental design

1. Sample size

   Describe how sample size was determined.

   No expected effect size was pre-specified. Generally accepted sample sizes were used.

2. Data exclusions

   Describe any data exclusions.

   NA

3. Replication

   Describe whether the experimental findings were reliably reproduced.

   every figure states how many times each experiment had been repeated. all the experiments were reliably reproduced

4. Randomization

   Describe how samples/organisms/participants were allocated into experimental groups.

   NA

5. Blinding

   Describe whether the investigators were blinded to group allocation during data collection and/or analysis.

   experiments were not performed blindly

   Note: all studies involving animals and/or human research participants must disclose whether blinding and randomization were used.

6. Statistical parameters

   For all figures and tables that use statistical methods, confirm that the following items are present in relevant figure legends (or the Methods section if additional space is needed).

n/a	Confirmed	
☐	☒	The exact sample size (*n*) for each experimental group/condition, given as a discrete number and unit of measurement (animals, litters, cultures, etc.)
☐	☒	A description of how samples were collected, noting whether measurements were taken from distinct samples or whether the same sample was measured repeatedly.
☐	☒	A statement indicating how many times each experiment was replicated
☐	☒	The statistical test(s) used and whether they are one- or two-sided (note: only common tests should be described solely by name; more complex techniques should be described in the Methods section)
☐	☒	A description of any assumptions or corrections, such as an adjustment for multiple comparisons
☐	☒	The test results (e.g. *p* values) given as exact values whenever possible and with confidence intervals noted
☐	☒	A summary of the descriptive statistics, including central tendency (e.g. median, mean) and variation (e.g. standard deviation, interquartile range)
☐	☒	Clearly defined error bars

See the web collection on statistics for biologists for further resources and guidance.

Software

Policy information about availability of computer code

7. Software

   Describe the software used to analyze the data in this study.

   flow jo, BD facsdiva, imagej, AIDA image analyzer

For all studies, we encourage code deposition in a community repository (e.g. GitHub). Authors must make computer code available to editors and reviewers upon request. The *Nature Methods* guidance for providing algorithms and software for publication may be useful for any submission.

Materials and reagents

Policy information about availability of materials

8. Materials availability

Indicate whether there are restrictions on availability of unique materials or if these materials are only available for distribution by a for-profit company.	all the materials are commercially available and material generated by us (KO cell lines, CMTM6 monoclonal antibodies) will be available upon request

9. Antibodies

Describe the antibodies used and how they were validated for use in the system under study (i.e. assay and species).	PD-L1, CMTM6, CMTM4, PD-L2 and STUB1 antibodies were validated by comparison of stain in wt and KO/KD cells

10. Eukaryotic cell lines

a. State the source of each eukaryotic cell line used.	sources of all the cell lines used is indicated in the methods section
b. Describe the method of cell line authentication used.	STR by source
c. Report whether the cell lines were tested for mycoplasma contamination.	yes, mycoplasma negative
d. If any of the cell lines used in the paper are listed in the database of commonly misidentified cell lines maintained by ICLAC, provide a scientific rationale for their use.	NA

Animals and human research participants

Policy information about studies involving animals; when reporting animal research, follow the ARRIVE guidelines

11. Description of research animals

Provide details on animals and/or animal-derived materials used in the study.	NA

Policy information about studies involving human research participants

12. Description of human research participants

Describe the covariate-relevant population characteristics of the human research participants.	NA

Corresponding Author: Ton Scumacher

Date: Jun 6, 2017

Flow Cytometry Reporting Summary

Form fields will expand as needed. Please do not leave fields blank.

Data presentation

For all flow cytometry data, confirm that:

☐ 1. The axis labels state the marker and fluorochrome used (e.g. CD4-FITC).

☒ 2. The axis scales are clearly visible. Include numbers along axes only for bottom left plot of group (a 'group' is an analysis of identical markers).

☒ 3. All plots are contour plots with outliers or pseudocolor plots.

☐ 4. A numerical value for number of cells or percentage (with statistics) is provided.

Methodological details

5. Describe the sample preparation.	cell lines or PDX cells were cultured, harvested by trypsin EDTA treatment. T cells were harvetsed and washed prior to stain. All cells were stained in PBS containing 0.5% w/v bovine serum albumin and 0.2% w/v sodium azide.
6. Identify the instrument used for data collection.	BD LSRII or Fortessa
7. Describe the software used to collect and analyze the flow cytometry data.	Data were collected using BD facsdiva and analyzed using flowjo
8. Describe the abundance of the relevant cell populations within post-sort fractions.	NA
9. Describe the gating strategy used.	Experiments were gated first by morphology to exclude cell debrees, then in case of not permeabilized cells by DAPI or PI negative.

Tick this box to confirm that a figure exemplifying the gating strategy is provided in the Supplementary Information. ☐